Exploring New Formate Dehydrogenase And Its Model Complex

グェン, ガー ティ タン

https://doi.org/10.15017/1500683

出版情報：九州大学, 2014, 博士（工学）, 課程博士
バージョン：
権利関係：全文ファイル公表済

Kyushu University
Graduate School of Engineering
Department of Chemistry and Biochemistry

Exploring New Formate Dehydrogenase And Its Model Complex

Nguyen Thi Thanh Nga

2015

CONTENTS

CONTENT OF FIGURES

CONTENT OF TABLES

CHAPTER 1

GENERAL INTRODUCTION

1.1. INTRODUCTION

The worldwide use of fossil fuels has given rise to vital problems of global warming, due to increasing atmospheric CO_2 concentration. Among various types of alternative energy sources, hydrogen is regarded as the most attractive clean energy carrier, which can provide carbon-free energy system. However, the current used H_2 is derived from fossil fuels, which does not lead to ultimate solutions of alternative clean energy problem and global warming. Therefore, new H_2 production methods have been required, but no significant methods have been developed.[1-4] I have focused on the exploitation of a new biological catalyst for formate activation and also a new hydrogenase model complex, which have formate hydrogenlyase for H_2 production, which may play important roles in development of renewable energy systems. Compared with H_2, formate is also favorable energy carrier as a non-flammable fuel for safe fuel cells system, enabling it to be easily stored and safely transported.[5-10]

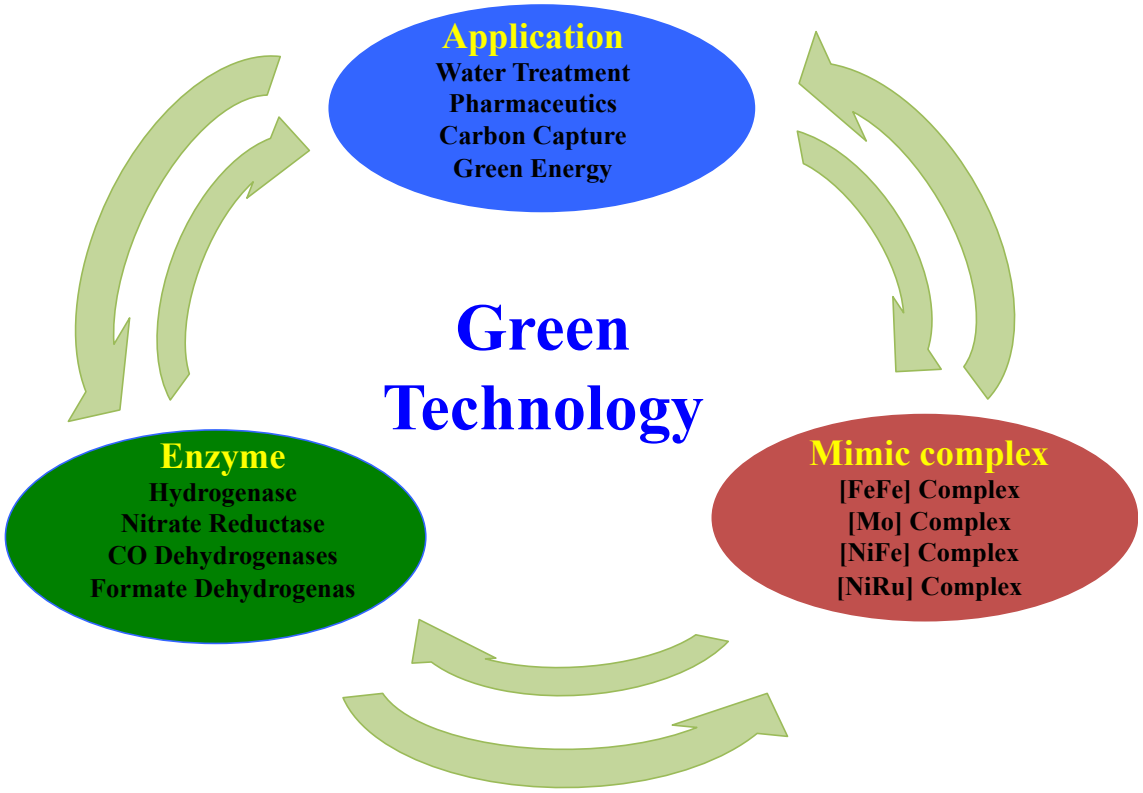

Figure 1.1 Harmonized system of biological and chemical catalysts for production of renewable energy.

Figure 1.1 is depicted in the relationship between enzyme and its biomimetic complex, and also their applications. Enzymes are highly attractive for industrial applications because of their highly specific recognition of specific substrates, leading to excellent selectivity.[11-13] However, most enzymes are required of the specific suitable reaction conditions such as pH and temperature, operating in the restrained conditions of pH between 5 and 10 and temperature between 20 and 50°C.[11] Therefore, we are actively paying attention to the development of biomimetic catalysts having high robustness and activity. The model complex inspired from biochemical studies of naturally occurring enzymes might have many advantages in the excellent selectivity of biological catalysts and the robustness of synthetic catalysts. In order to create a new effective biomimetic catalyst, the exploring new enzyme and its biochemical

characterization using homogeneously purified enzyme are necessary to assess the ability of enzyme, providing new insight into the development of effective biomimetic model studies.[14-16] For examples, hydrogenase, which catalyzes the activation of H_2 into two protons (H^+) and two electrons (e^-), and its mimic model are the good examples of the harmonized system of biological and chemical catalysts for production of renewable energy.[14,15] Indeed, Ogo group found a new membrane-bound hydrogenase (MBH) having a remarkable O_2-stability along with a high H_2-activation.[17] In a polymer electrolyte fuel cell (PFEC) system, the ability of MBH surpasses platinum as an anode electrode for H_2 oxidation.[18] They also succeeded in it's synthetic model complexes of a Ni(μ-H)Ru complex {[Ni^{II}L(μ-H)Ru^{II}(η^6-C_6Me_6)], L = *N,N'*-dimethyl-3,7-diazanonane-1,9-dithiolato} and [NiFe] complex (Ni^{II}(X')Fe^{II}(MeCN){$P(OEt)_3$}$_3$)$(BPh_4)_2$, which X' = *N,N'*-diethyl-3,7-diazanonane-1,9-dithiolato, Et indicates an ethyl group, and Ph a phenyl group).[19,20] The [NiRu] complexes also have catalytic abilities for H_2 activation in water at ambient conditions, applying in the PEPC as anode catalysts.[21] Thus, the original concept of this research is to create the fusion technology by developing useful biological- and chemical- catalysts into the ideal system, which can be used as an energy generator to produce "H_2" or activation of "formate".

1.2. ARRANGEMENT OF THESIS

To achieve the goal, this thesis is described in the Chapter 2 of purification and characterization a new formate dehydrogenase from our newly isolated bacterium *Citrobacter* sp. S-77. In the Chapter 3, I have attempted to create the model complex of formate hydrogenlyase with the modified [NiFe]H_2ase model complex.

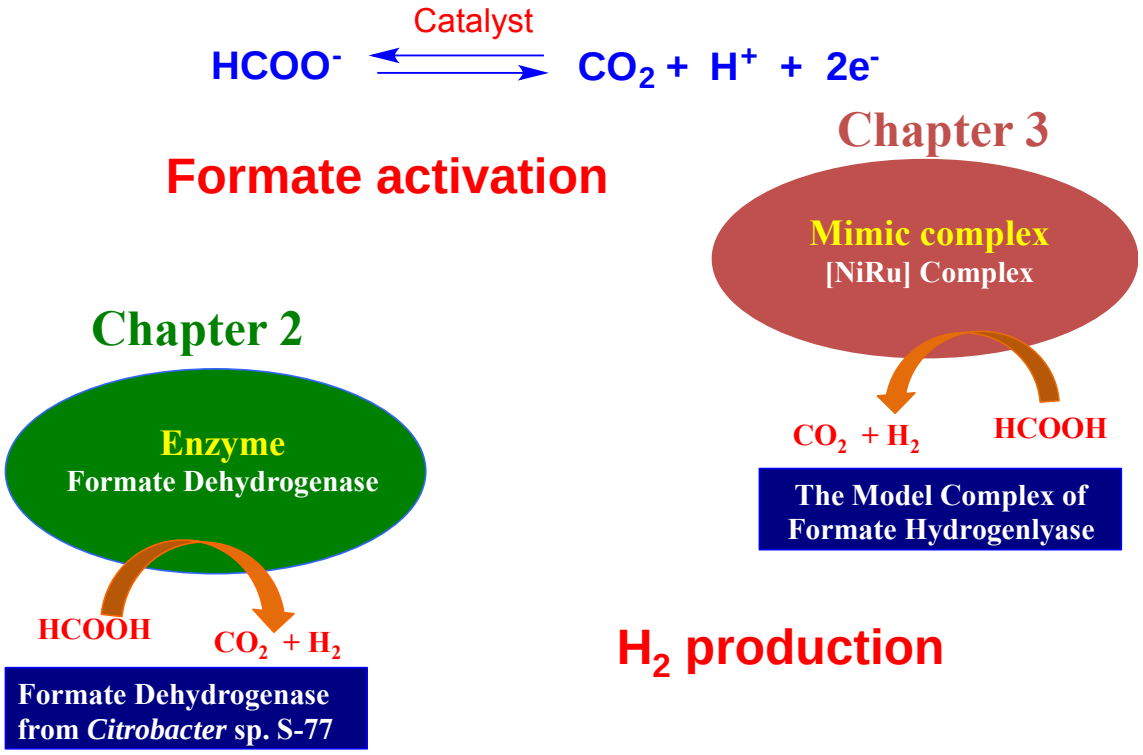

Figure 1.2 The arrangement of thesis

Formate is an important energy carrier that can generate electrons or produce H_2 by catalytic reaction of biological and chemical catalysts. The metalloenzyme of FDH catalyze the oxidation of formate, which plays an important role in electron transfer pathway in aerobic and anaerobic respirations.[22,23] In order to understand the mechanism of formate oxidation, the Chapter 2 is the first effort to define the biochemical characterization of a new formate dehydrogenase from our newly isolated bacterium *Citrobacter* sp. S-77. On the other hand, owing to the O_2-sensitivity of H_2 production from formate by biological reaction, the system is not well established. Therefore, I developed a new NiRu complex catalyzing H_2 production from formic acid, which is the same as the catalytic reaction of formate hydrogenlyase. (Figure 1.2)

In Chapter 1, I attempt to provide the general information of purposed of my thesis, and also FDH and the model research described in this thesis.

In Chapter 2, I describe the purification procedure and biochemical characterization of new formate dehydrogenase from *Citrobacter* sp. S-77 (FDH_{S77}). The purified FDH_{S77} is a molybdenum-containing membrane-bound FDH having high thermostability, pH resistance, and O_2-stability. The Michaelis-Menten constant, electrochemical analysis, and EPR and UV-visible spectra are also described in the Chapter 2.

In **Chapter** 3, the development of a mimic [NiFe]hydrogenase complex [(μ-hydro)(format)$Ni^{II}Ru^{II}$] is presented. The model complex can display the same reaction of a formate hydrogenlyase, heterolytically splitting dihydrogen into protons and electrons and decomposing formic acid into H_2 and CO_2. The crystal structure of (μ-hydrido)(formato)$Ni^{II}Ru^{II}$ and the reaction intermediate of the (μ-hydro)(formato)$Ni^{II}Ru^{II}$ complex are defined.

In **Chapter** 4, I discuss the new knowledge obtained in these studies that may provide new insight for the development of highly efficient new catalysts for future technology.

REFERENCES

1. **Veziroğlu, T. N and Şahin, S.**: 21st Century's energy: Hydrogen energy system, Energ. Convers. Manage., **49**, 1820-1831 (2008).
2. **Dutta S.**: A review on production, storage of hydrogen and its utilization as energy resource, J. Ind. Eng Chem., **20**, 1148-1156 (2014).
3. **Balat, M.**: Potential importance of hydrogen as a future solution to environmental and transportation problem, Int. J. Hydrogen Energy, **33**, 4013-4029 (2008).
4. **Mazloomi, K. and Gomes, C.**: Hydrogen as an energy carrier: Prospects and challenges, Renew Sust Energ Rev., **16**, 3024-3033 (2012).
5. **Joó, F.**: Breakthroughs in hydrogen storage- formic acid as a sustainable storage material for hydrogen, ChemSusChem, **1**, 805-808 (2008).
6. **Zaidman B., Wienwe H., and Sasson Y.**: Formate salts as chemical carriers in hydrogen storage and transportation, Int. J. Hydrogen Energy, **11**, 341-347 (1986).
7. **Graseman M. and Laurency G.**: Formic acid as a hydrogen source- recent developments and future trends, Energy Environ. Sci., **5**, 8171-8181 (2012).
8. **Yu, X. and Pickup, P. G.**: Recent advances in direct formic acid fuel cells (DFAFC), J. Power Sources, **182**, 124-132 (2008).
9. **Enthaler, S., Langermann, J. V., and Schmidt, T.**: Carbon dioxide and formic acid-the couple of environmental-friendly hydrogen storage? Energy Environ. Sci., **3**, 1207-1217 (2010).
10. **Leitner, W.**: Carbon dioxide as a raw material: the synthesis of formic acid and its derivatives from CO_2. Angew. Chem. Int. Ed. Engl., **34**, 2207-2221 (1995).
11. **Schmid, A., Dordick, J. S., Hauer, B., Kiener, A., Wubbolts, M., and Witholt, B.**: Industrial biocatalysis today and tomorrow, Nature, **409**, 258-268 (2001).

12. **Kirk, O., Borchert, T. V., and Fuglsang, C. C.**: Industrial enzyme application, Curr. Opin. Chem. Biol., **13**, 345-351 (2002).
13. **Beilen, J. B.v. and Li, Z.**: Enzyme technology: an overview, Curr. Opin. Chem. Biol., **13**, 338-344 (2002).
14. **Bouwman, E. and Reedijk, J.**: Structural and functional models related to the nickel hydrogenases, Coord. Chem. Rev., **249**, 1555-1581 (2005).
15. **Simmons, T. R., Berggen, G., Bacchi, M., Fontecave, M., and Artero, V.**: Mimicking hydrogenases: From biomimetics to artificial enzymes, Coord. Chem. Rev., **270-271**, 127-150 (2014).
16. **Appel, A. M., Bercaw, J. E., Bocarsly, A. B., Dobbek, H., DuBois, D. L., M. Dupuis, Ferry, J. G., Fujita, E., Hille, R., Kenis, P. J. A., Kerfeld, C. A., Morris, R. H., Peden, C. H. F., Portis, A. R., Ragsdale, S. W., Rauchfuss, T. B., Reek, J. N. H., Seefeldt, L. C., Thauer, R. K., and Waldrop, G. L.**: Frontiers, opportunities, and challenges in biochemical and chemical catalysis of CO_2 fixation, Chem. Rev., **113**, 6621–6658 (2013).
17. **Eguchi, S., Yoon, K.-S., and Ogo, S.**: O_2-stable membrane-bound [NiFe]hydrogenase from a newly isolated *Citrobacter* sp. S-77, J. Biosi. Bioeng., **114**, 479-484 (2012).
18. **Matsumoto, T., Eguchi, S., Nakai, H., Hibino, T., Yoon, K.-S., and Ogo, S.**: [NiFe]Hydrogengase from *Citrobacter* sp. S-77 surpasses platinum as an electrode for H_2 oxidation reaction, Angew. Chem. Int. Ed., **53**, 8895-8898 (2014).
19. **Ogo, S., Kabe, R., Uehara, K., Kure, B., Nishimura, T., Menon, S. C., Harada, R., Fukuzumi, S., Higuchi, Y., Ohhara, T., Tamada, T., and Kuroki, R.**: A Dinuclear Ni(μ-H)Ru complex derived from H_2, Science, **316**, 585–587 (2007).

20. **Ogo, S., Ichikawa, K., Kishima, T., Matsumoto, T., Nakai, H., Kusaka, K., and Ohhara, K.**: A functional [NiFe]hydrogenase mimic that catalyzes electron and hydride transfer from H_2, Science, **339**, 682–684 (2013).
21. **Matsumoto, T., Kim, K., and Ogo, S.**: Molecular catalysis in a fuel cell, Angew. Chem. Int. Ed., **50**, 11202-11205 (2011).
22. **Leohartsberger, S., Korsa, I., and Böck A.**: The molecular biology of formate metabolism in *Enterobacteria*, J. Mol. Microbiol. Biotechnol., **4**, 269-276 (2002).
23. **Sawers, R. G.**: Formate and its role in hydrogen production in *Escherichia coli*, Biochem. Soc. Trans., **33** (2005).

CHAPTER 2

PURIFICATION AND CHARACTERIZATION OF A MOLYBDENUM-CONTAINING MEMBRANE-BOUND FORMATE DEHYDROGENASE FROM *CITROBACTER* SP. S-77

ABSTRACT

Membrane-bound formate dehydrogenase (FDH) was purified from a newly isolated bacterium, *Citrobacter* sp. S-77. By gel filtration analysis of the FDH from *Citrobacter* sp. S-77 (FDH_{S77}), it was a monomer with molecular mass of approximately 150 kDa. The purified FDH_{S77} showed as three different protein bands with molecular mass of approximately 95, 87, and 32 kDa, respectively, on SDS-PAGE. According to the N-terminal amino acid sequence analysis, the sequence alignment of 87 kDa protein band was identical to that of the large subunit of 95 kDa, indicating that the purified FDH_{S77} consisted of two subunits; a 95 kDa large subunit and a 32 kDa small subunit, The purified FDH_{S77} was not contained a heme *b* subunit. The specific activity of FDH_{S77} was determined as the V_{max} of 30.4 U/mg using benzyl viologen as an electron acceptor. The EPR and ICP-MS spectra indicate that the FDH_{S77} is a molybdenum-containing enzyme, displaying a remarkable O_2-stability along with thermostability and

pH resistance. This is the first report of the purification and characterization of a FDH from *Citrobacter* species.

2.1. INTRODUCTION

Biological carbon dioxide conversion is extremely important process for all organisms, which is very closely linked to the flow of energy that is maintained by living organisms in the biosphere. Organisms that use CO_2 as a carbon source may be employed to produce useful compounds that related to the biological production of energy from redox or electron transport proteins, such as photosynthetic reaction centers, hydrogenase, formate dehydrogenase (FDH), puruvate ferredoxin oxidoreductase, CO dehydrogenase, and so on.[1-3] Among them, FDH is one of the most attractive metalloenzyme that catalyzes the reversible oxidation of formate to two-electrons and CO_2 (equation 2.1). [2,4,5]

$$HCOO^- \xrightleftharpoons{FDH} CO_2 + 2e^- + H^+ \qquad \text{(Eq. 2.1)}$$

The FDH has also a great potential for use as a useful biocatalyst in biotechnological application, such as for the regeneration of cofactors of NAD(P)H in the pharmaceutical industry[6] and for an effective homogeneous, formate-oxidation biocatalyst in safe fuel cell systems. In addition, FDH has also a great potential as an effective biocatalyst for conversion of CO_2 to make formate as an alternative fuel.[7] However, the enzyme is very sensitive to O_2, which can easily loss of its catalytic activity after air oxidation.[2,4,5,8-10] The O_2-sensitivy of the FDH is considered as a major bottleneck to practical use of the enzyme in its biotechnological application.

Table 2.1 Summaries of formate dehydrogenases

	FDH-H[10]	FDH-N[9]	FDH-O[8]	W-FDH[11]
Microorganisms	*E. coli*	*E. coli*	*E. coli*	*D. gigas*
Location	cytoplasm	membrane	membrane	periplasm
Subunit (kDa)	70	110, 32, 20	110, 35, 25	92, 29
Metal cofactors	[4Fe-4S], Mo, Se	[4Fe-4S], Mo, Se	-	[4Fe-4S], W, Se

So far, a number of FDH have been purified from various microorganisms, which are divided into four groups based on their physiological function, protein structure, and on their metal components in the active site (Table 2.1): FDH-H, FDH-N, FDH-O, and W-FDH. FDHs contain metal cofactors of molybdenum or tungsten in the active site, which are similar structures to each other.[12-14] Although the active site of FDHs displays the structural similarity, but those of containing cofactors and subunit compositions are varied. FDH-H is a part of the protein complex of formate hydrogenlyase.[8,15] FDH-O has high levels of sequence similarity with FDH-N, but the purification and biochemical characterization of FDH-O has not been performed. Therefore, the biochemical properties of FDH-O have not been understood. W-FDH is mainly located in the cytoplasm, which was purified and determined the crystal structure from *Desulfovibrio gigas*.[14] Most FDHs contain metal cofactors of molybdenum or tungsten in their active sites.[2,5,10-14] Among them, FDH-N from *Escherichia coli*, which is an analogous the FDH purified from *Citrobacter* sp. S-77 (FDH_{S77}), was purified and characterized.[9,13] The crystal structural of the FDH-N was determined at 1.6 Å, containing a selenium atom that is coordinated to molybdenum of the molybdopterin (MTP) moieties in the active site (Figure 2.1).[13] The FDH-N from

E. coli is highly stable under anaerobic conditions, but the enzyme is very sensitive to aerobic conditions.[9]

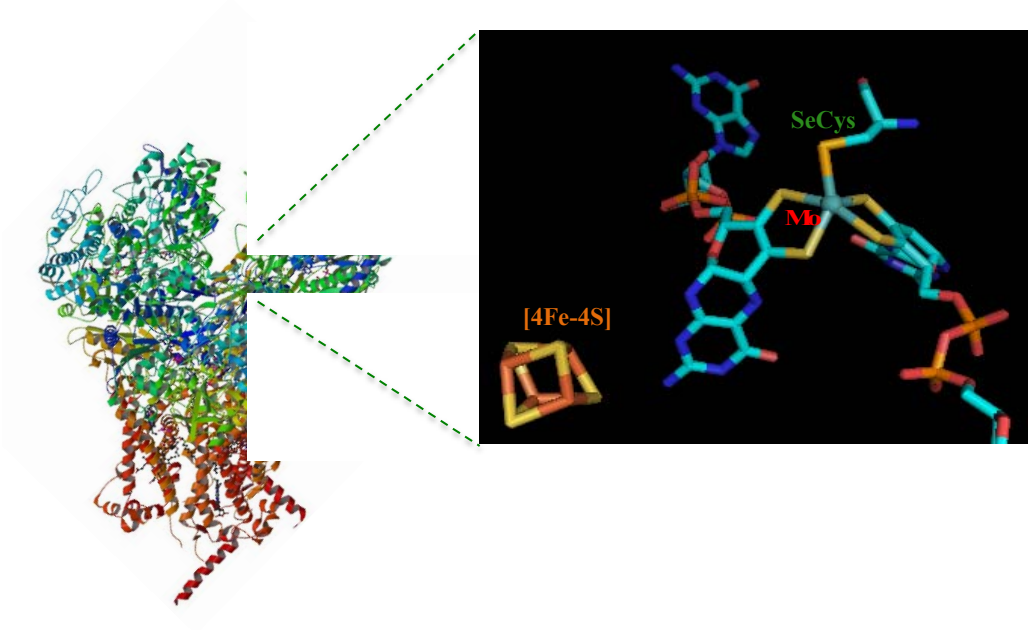

Figure 2.1 The crystal structure and the active site of FDH-N (1KQF)

During the course of exploring novel biocatalysts, we have found an O_2-stable membrane- bound FDH from the recently isolated bacterium, *Citrobacter* sp. strain S-77.[16,17] Although the FDH activity was measured in the cell extracts of *C. amalonaticus*[18] and *C. freundii*,[19] the purification and characterization of FDH from the bacteria, however, has not been reported. Here, we report the first purification and characterization of a molybdenum containing FDH from the genus of *Citrobacter*. Like the MBH from *Citrobacter* sp. S-77, the purified FDH_{S77} displays a remarkable O_2-stability, along with thermostability and a wide range of pH resistance. This newly found O_2-stable FDH_{S77} might be an important enzyme that may significantly contribute to the development of effective biocatalysts for CO_2 conversion.

2.2. MATERIAL AND METHODS

2.2.1. Growth conditions

Citrobacter sp. strain S-77 isolated from Aso-Kuju National Park, Oita, Japan was cultivated aerobically at 30°C in a modified Bacto marine broth medium.[16] The mass culture was carried out in 20 L Carboy bottles containing 15 L the following components in the Table 2.2. In order to express FDH activity, the metal additional components of 0.1 μM Na_2WO_4, 0.1 μM Na_2MoO_4, and 0.2 μM $Na_2Se_2O_3$ were added into the previously prepared medium. The growth cells after culture for 4 days were harvested by centrifugation at 9,000 × *g* for 20 min. The precipitated pellet was frozen in liquid N_2 and stored at -80°C.

Table 2.2 Growth medium of *Citrobacter* sp. S-77

Components	weight (g/L)
Yeast extract	3.0
Peptone	3.0
$(NH_4)_2SO_4$	3.0
$MgSO_4.7H_2O$	0.5
K_2HPO_4	2.0
KH_2PO_4	1.0
Ammonium iron (III) citrate	0.2
$CaCl_2$	0.1
Sodium formate	2.0
D-glucose	1.0

2.2.2. Enzyme assay of FDH

FDH activity was routinely determined spectrophotometrically by following the formate-dependent reduction of benzyl viologen (BV) at 30°C in glass cuvettes sealed with a rubber stopper and an aluminum cap under strictly anaerobic conditions. In order to maintain strictly anaerobic conditions for enzyme assay, all assays were performed under strictly anaerobic conditions by flushing with a constant flow of N_2 for 5 min using a vacuum gas manifold. The standard assay mixture contained 10 mM BV in 50 mM 3-(N-morpholino)propanesulfonic acid (MOPS) buffer, pH 7.0. Activity was calculated by the increase in absorbance of BV at 600 nm ($\varepsilon_{600\,nm}$ = 8.3 mM^{-1} cm^{-1}).[20] The maximal kinetic velocity (V_{max}) and K_m values were determined by fitting the data to the Michaelis-Menten equation using nonlinear regression. The data were analyzed by using the Enzyme Kinetics Module1.1 of SigmaPlot 8.0 software (Jandel Scientific, CA). Activity was expressed as units/mg of protein, where one unit (U) is equivalent to oxidation of 1 μmol formate/min.

2.2.3. Isolation of membrane fraction

Frozen cells (70.0 g) was suspended in 20 mM MOPS buffer (pH 7.0) and disrupted by sonication four times for 2 min in ice bath at 60 W with an Ultrasonic Disruptor UD-200 (TOMY SEIKO Inc., Japan). The broken cells were centrifuged at 3,000 × *g* for 20 in to remove cell debris and membrane was precipitated by ultracentrifugation (Optima L-90K, Beckman Coulter Inc., USA) at 150,000 × *g* for 1 h at 4°C. The membrane was washed one with the same buffer containing 1 M NaCl to remove cytoplasmic contaminants bound in membrane.

2.2.4. Solubilization of FDH from the isolated membrane

The washed membrane were suspended to be 4 mg/mL protein concentration in 20 mM MOPS (pH 7.0) containing 1.0 M NaCl and 1 mM dithiothreitol (DTT). FDH was solubilized by adding of 0.5% Sulfobetaine 3-12 (SB3-12) of zwitterionic detergent. Immediately after addition of the detergent, the membrane solution was slowly stirred at 4°C for 3 h under 100% N_2 gas. The extract was then centrifuged at 150, 000 × *g* for 1h. The supernatant was used for purification of FDH.

2.2.5. Purification of FDH

All purification procedures were carried out at room temperature under strictly anaerobic conditions using a Coy anaerobic chamber under an atmosphere of 98% N_2 and 2% H_2. Protein purification was performed in the Coy anaerobic chamber using an AKTA-FPLC system (GE Healthcare) as following process. All buffers were repeatedly degassed and flushed with N_2 and were stored in the anaerobic chamber.

2.2.5-1. Hydroxyapatite

The solubilized membrane proteins were directly loaded onto hydroxyapatite (2.5 × 15 cm; Bio-Rad Laboratories Inc.), pre-equilibrated with 1 mM potassium phosphate (KP) buffer (pH 7.0) containing 0.5 mM DTT and 0.2% SB3-12 at a flow rate of 8.0 mL/min. FDH activity was detected around 50 mM concentration of KP by a linear gradient between 1-100 mM KP buffer.

2.2.5-2. Q Sepharose high performance

The active pools of FDH after hydroxyapatite were directly applied onto a Q Sepharose HP (1.6 × 12 cm. GE Healthcare, UK) pre-equilibrated with 20 mM Tris buffer (pH 8.0) containing 1 mM DTT and 0.2% SB3-12. After loading the sample the column was washed with the same buffer and the protein was eluted with a gradient of 0.1-0.35 M NaCl at a flow rate of 4.5 mL/min.

2.2.5-3. Resource 15 Q

The FDH eluted at approximately 0.3 M NaCl by Q Sepharose HP was diluted 3-fold with nonsalt buffer and applied onto a Resource 15 Q (0.64 × 3 cm; GE Healthcare, UK). After sample application, the column was washed with wash buffer and then eluted isocratically using a buffer containing 0.2 M NaCl, followed by a gradient of buffer containing 0.25 to 0.4 M NaCl at a flow rate of 1.5 mL/min. At this stage, the FDH eluted at approximately 0.32 M NaCl.

2.2.5-4. Superdex 200

The FDH fraction was concentrated using Amicon Ultra-15 (30,000 NMWL; Millipore Corp., Billerica, MA) and then loaded onto a Superdex 200 column (1.6 × 50 cm; GE Healthcare, UK) pre-equilibrated with 10 mM Tris-HCl buffer (pH 8.0) containing 0.3 M NaCl and 0.2% SB3-12 at a flow rate of 1.0 mL/min, eluting as a single peak with a molecular weight of approximately 150 kDa.

2.2.6. Gel electrophoresis

Protein purity was established by SDS-PAGE and Native-PAGE analysis using a 5-20% gradient gel. The molecular weight was calculated from a standard linear regression curve using low range-standard proteins (M_rs, 14,000 to 94,000) of Bio-Rad. Activity staining in the nondenaturating gel was carried out in the presence of 10 mM formate and 1 mM triphenyl tetrazolium chloride as an electron acceptor in 50 mM MOPS buffer (pH 7.0) at 30°C under N_2 gas.

2.2.7. Oxygen stability of the purified FDH_{S77}

In order to evaluate O_2-stability of the purified FDH_{S77}, the formate-oxidation activity of the air oxidized enzyme after exposure to air was assayed. The vials containing the purified enzyme solution were flushed with dry air for 5 min and then the enzyme was oxidized by incubation under O_2 at 4°C. The remaining activity of the oxidized enzyme was measured periodically. The atmosphere in the assay cuvettes sealed with a gas-tight rubber stoppers and an aluminum caps was exchanged by flushing with a constant flow of N_2 for 5 min to remove the dissolved trace O_2 in the reaction solution and then the assay was initiated by injection of the enzyme solution.

2.2.8. Effect of pH on FDH activity

For the optimum reaction pH measurement, the Britton-Robinson (BR) universal buffer (pH 5.0–9.0) was used. The optimum pH for the reaction was determined by measuring the activity using a 50 mM Britton–Robinson (BR) buffer system. For the pH stability, the purified FDH_{S77} was incubated in the same BR buffer over a wide pH range (3.0–10.0) at 4°C under N_2. The pH stability of the enzyme was determined by

measuring the residual activity after incubation for 3 h.

2.2.9. Thermal properties of the FDH_{S77}

The optimum reaction temperature was determined by measuring the formate oxidation activity over a temperature range of 20–100°C. Before injection of the enzyme solution, the reaction mixture containing 10 mM BV was pre-incubated for 10 min under N_2 at each measuring temperature. For the thermostability of the purified FDH_{S77}, the enzyme solution (0.1 mg/mL) in a 10 mM Tris-HCl buffer (pH 8.0) containing 0.3 M NaCl and 0.2% SB3-12 was incubated between 0 and 80°C for 20 min under N_2. The denatured protein was then removed by centrifugation at 14,000 × *g* for 20 min and subjected to the enzyme assay. The thermostability was determined by measuring the remaining activity after thermal incubation.

2.2.10. Electrochemical experiments

The amperometric *i-t* curve measurement was used to determine O_2-stability of the FDH_{S77}. The amperometric *i-t* curve was performed with a computer controlled electrochemical analyzer (CH Instruments model 760 DT, BAS Inc., Japan) connected to a rotating ring/disk electrode device (RRDE-3, BAS Inc.). An Ag/AgCl/3.0 M NaCl electrode (assumed + 0.197 V vs. SHE; model RE-1B, BAS Inc.) was used as a reference electrode. A platinum wire was used as a counter electrode. A glassy carbon disk-working electrode (3 mm in diameter, BAS Inc.) was carefully polished with 0.05 μm alumina/water slurry on a glass-plate mounted microcloth pad and the polished electrode was rinsed with distilled water. Electrochemical measurements were carried out at 30°C by purging the electrolysis cell with N_2 gas or dry air. The reaction mixture

(10 mL) contained 200 μg of the purified enzyme, 20 mM formate, 2 mM BV, and 0.2 M NaCl in 50 mM Tris-HCl buffer (pH 8.0). The temperature of the reaction chamber was controlled by a water jacket.

2.2.11. EPR and UV-visible spectra

X-band electron paramagnetic resonance (EPR) spectra were measured by a JEOL JES-FA200 spectrometer. The air-oxidized and formate-reduced samples were injected into 3-mm-diameter quartz EPR tubes and frozen by slowly immersing the tubes into liquid nitrogen. The formate-reduced enzyme was prepared by promoting the FDH reaction under N_2 for 20 min at 30°C, and then injected into EPR tubes sealed with a rubber stopper. EPR spectra were measured at 110 K under liquid nitrogen. UV-visible spectra were measured using a JASCO spectrophotometer (Jasco, Tokyo, Japan).

2.2.12. N-terminal analysis

The N-terminal amino acid sequence of each subunit of the purified enzyme was determined by the automated Edman degradation system of ABI protein sequencer 473A (Applied Biosystems Japan, Tokyo). Each subunit of the enzyme was separated by SDS-PAGE and then blotted onto a polyvinylidene difluoride membrane.[21]

2.2.13. Other methods

The protein concentration was measured using established procedures for the Bio-Rad DC Protein Assay (Bio-Rad Laboratories Inc.).[22] The Mo, W, Se, and Fe contents of the purified enzyme were analyzed by an inductively coupled plasma mass spectrometer (ICP-MS) using an Agilent 7500c (Agilent Technologies, Inc., USA). The

molecular weight of the purified enzyme was determined by gel filtration using a Superose 12 column calibrated with standard molecular weight markers (Bio-Rad Laboratories Inc.).

2.3. RESULTS

2.3.1. Solubilization of the FDH_{S77} from isolated membrane

In order to express FDH activity, I added the additional components of 2.0 g/L sodium formate, 1.0 g/L D-glucose, and metal components of 0.1 μM Na_2WO_4, 0.1 μM Na_2MoO_4, and 0.2 μM $Na_2Se_2O_3$ into the previously described medium. In this modified medium, sodium thiosulfate was removed the initial medium described.[16] From the harvested cells, the cytoplasmic membrane fraction was prepared by ultracentrifugation. The isolated membrane fraction of *Citrobacter* sp. strain S-77 was contained a significant FDH activity. The FDH_{S77} could be effectively solubilized by the zwitterionic detergent of 0.5% SB3-12, which could be recovered to approximately 87% of total FDH activity from the membrane fraction of the strain S-77.

2.3.2. Purification of the FDH_{S77} from solubilized membrane fraction

In the first purification step of the FDH_{S77}, I used a hydroxyapatite column, which could be effectively separated the FDH_{S77} from many other membrane proteins, particularly in the majority of hydrogenase activity. Through subsequent column chromatographies of Q Sepharose high performance, Resource 15 Q, and Superdex 200, the FDH_{S77} was purified to electrophoretic homogeneity. The purified FDH_{S77} on SDS-PAGE gel appeared as three distinct protein bands, estimated to be approximately 95, 87, and 32 kDa, respectively (Figure 2.2).

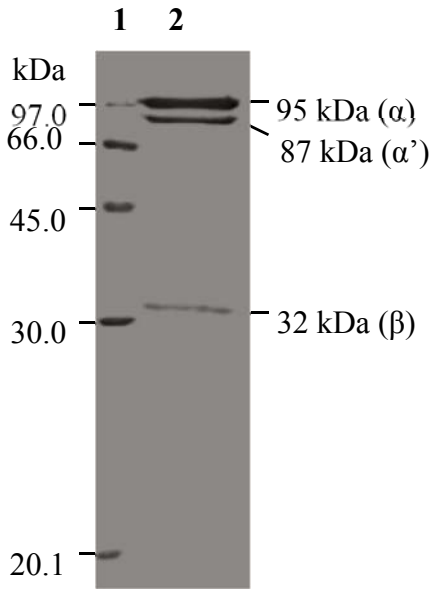

Figure 2.2 SDS-PAGE (12.5%) gel of the purified FDH_{S77}. Lane 1, low-molecular weight standard proteins (M_rs, 14,000 – 97,000); lane 2, 5 μg of the purified FDH_{S77}.

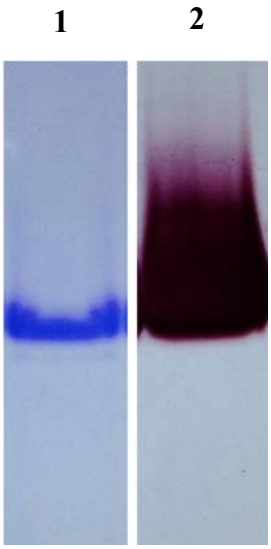

Figure 2.3 Native –PAGE (5-20% gradient) analysis of the purified FDH_{S77}, Lane 1, protein stain of the purified FDH_{S77}, lane 2, activity stain of the purified FDH_{S77}.

However, according to the results of N-terminal amino acid sequence analysis, the initial amino terminal sequence of the 95 kDa subunit is identical to that of the 87 kDa polypeptide, suggesting that the 87 kDa protein is a degraded product of the large subunit. As shown in Figure 2.5, the initial 19 amino acid residues (blue color) determined for the FDH_{S77} is the same for that of the FDH-N from *E. coli* (Figure 2.4). In addition, the purified FDH_{S77} gave a single protein band on a nondenaturating gel, which was responsible for the activity band of FDH_{S77} (Figure 2.3).

FDH_{S77} (α) from S-77	QARNYKLLRAKEIRNTCTY
FDH_{S77} (α')from S-77	QARNYKLLRAKEIRNTCTY
FDH-N (α) from *E. coli*	QARNYKLLRAKEIRNTCTY
FDH-O (α) from *E. coli*	ETRQYKLLRTRETRNTCTY
FDH (α) from D. *gigas*	ATMALKTVDAKQTTSVCCY
FDH-H from *E. coli*	MKKVVTVCPY
FDH_{S77} (β) from S-77	SMETQDIIKRSATNSITPP
FDH-N (β) from *E. coli*	AMETQDIIKRSATNSITPP
FDH-O (β) from *E. coli*	AYQSQDIIRRSATNGLTPA
FDH (β)(D.*gigas*)	SKGFFVDTTRCTACRGCQV

Figure 2.4 Comparison of N-terminal amino acid sequences of FDH. The sequences of FDH_{S77} were determined in this study. The sequences from other FDHs were extracted from protein dataset of NCBI (www.ncbi.nlm.nih.gov)

Large-subunit

```
1       MDVSRRQFFK ICAGGMAGTT VAALGFAPKM ALAQARNYKL LRAKEIRNTC      50
51      TYCSVGCGLL MYSLGDGAKN AKESIYHIEG DPDHPVSRGA LCPKGAGLLD     100
101     YVHSENRLRY PEYRAPGSDK WQRISWDEAF SRIAKLMKAD RDANFIEKNE     150
151     QGVTVNRWLS TGMLCASAAS NETGMLTQKF VRSLGMLAVD NQARVHGPTV     200
201     ASLAPTFGRG AMTNHWVDIK NANVVMVMGG NAAEAHPVGF RWAMEAKNNN     250
251     DATLIVVDPR FTRTASVADI YAPIRSGTDI TFLSGVLLYL IENNKINAEY     300
301     VKHYTNASLL VRDDFAFEDG LFSGYDAKKR QYDKSSWNYQ FDENGYAKRD     350
351     ETLSHPRCVW NLLKQHVSRY TPDVVENICG TPKADFLKVC EVLASTSAAD     400
401     RTTTFLYALG WTQHTVGAQN IRTMAMIQLL LGNMGMAGGG VNALRGHSNI     450
451     QGLTDLGLLS TSLPGYLTLP SEKQADLQTY LAANTPKATL AEQVNYWGNY     500
501     PKFFVSLMKS FYGNAAQKEN DWGFEWLPKW DQSYDVIKYF NMMDSGKVTG     550
551     YICQGFNPVA SFPDKNKVVQ SLSKLKYLVI IDPLVTETST FWQNHGDSND     600
601     VDPASIQTEV FRLPSTCFAE EDGSIANSGR WLQWHWKGQD APGEARNDGE     650
651     ILAGIYHRLR EMYRTEGGKG VEPVLKMSWN YKQPDEPHSE EVAKENNGYA     700
701     LEDLYDANGV LVAKKGQLLN SFALLRDDGT TASSCWIYTG SWTEQGNQMA     750
751     NRDNADPSGL GNTLGWAWAW PLNRRVLYNR ASADPQGKPW DPKRMLIKWN     800
801     GTKWTGNDIP DFNNAAPGSG TNPFIMQPEG LGRLFAIDKL AEGPFPEHYE     850
851     PMETPLGTNP LHPNVISNPA ARLYEADALR MGNKQDFPYV GTTYRLTEHF     900
901     HTWTKHALLN AIAQPEQFVE ISETLAAAKG IANGDYVKVS SKRGFIRAVA     950
951     VVTRRLRTLH VNGQQVETVG IPIHWGFEGV ARKGFIANTL TPNVGDANSQ    1000
1001    TPEYKAFLVN IEKA                                        1014
```

Figure 2.5 Amino acid sequence alignments of the large subunits of FDH_{S77}. The large subunit of the FDH_{S77} contains a signal sequence of twin-arginine transport (Tat) (red color), the determined N-terminal sequence from the purified FDH_{S77} (blue color). The cysteine residues of iron-sulfur-cluster-binding motifs ($CX_{2-3}CX_3CX_{26-34}C$) are given in bold letter, which is typical [4Fe-4S] cluster.

Small-subunit

```
1       MSMETQDIIK RSATNSITPP PQARDYKAEV AKLIDVSTCI GCKACQVACS      50

51      EWNDIRDEVG HCVGVYDNPA DLSAKSWTVM RFTETEQNGK LEWLIRKDGC     100

101     MHCEDPGCLK ACPSAGAIIQ YANGIVDFQS EHCIGCGYCI AGCPFNIPRL     150

151     NKEDNRVYKC TLCVDRVSVG QEPACVKTCP TGAIHFGTKQ EMLEMAEQRV     200

201     EKLKARGFEH AGVYNPQGVG GTHVMYVLHH ANQPELYHGL PKDPQIDTSI     250

251     NLWKGALKPL AAAGFIATFA GLIYHYIGIG PNKEVDDDEE DHHE           294
```

Figure 2.6 Alignment of the amino acid sequences of the small-subunit of FDHS77. The determined N-terminal sequence from the purified FDHS77 was marked as a blue color.

2.3.3. The molecular weight determination of the FDHS77

The purified FDHS77 exhibited a single UV-absorption peak of the gel filtration column of Superdex 200 (Figure 2.7A). Subsequent experimental results showed that the molecular weight of the native enzyme, determined by Superose 12 gel filtration was estimated to be approximately 150 ± 20 kDa (Figure 2.7B). Taken together, we have concluded that the 87 kDa polypeptide is a degradation byproduct of the 95 kDa polypeptide of large subunit. The large subunit of FDHS77 appears to be easily cleaved in the C-terminal region during the step of purification or the development of SDS-PAGE analysis. Based on amino acid comparison of other bacterial FDHs, the sequences of FDHS77 have high homology with those of FDH-N from *E. coli*, suggesting that operon structure of the FDH genes of *Citrobacter* sp. S-77 may encode in the *fdnGHI* operon.[5] The operon of FDH-N from *E. coli* encodes three different polypeptides of approximately 110, 32, and 20 kDa.[9]

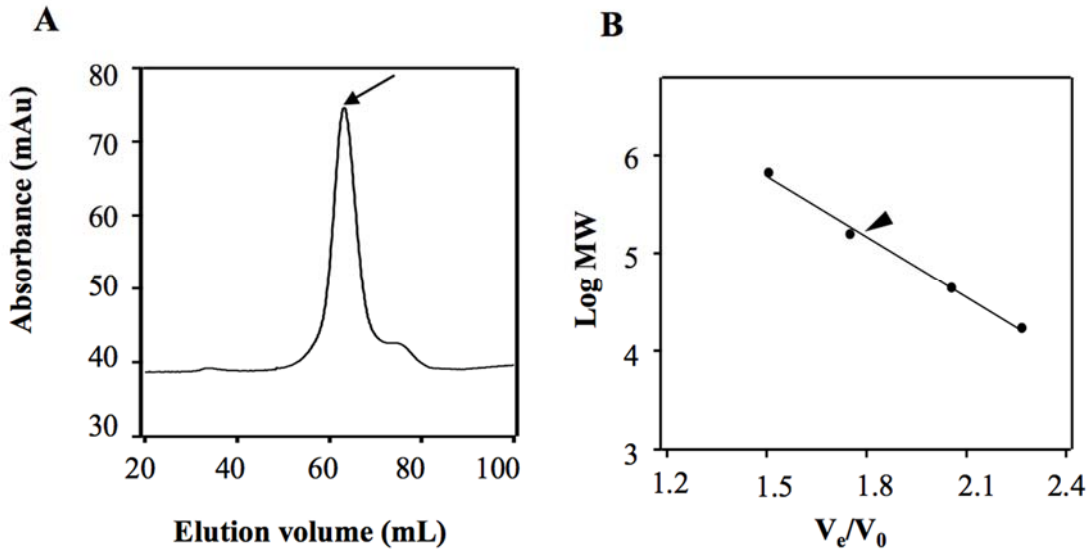

Figure 2.7 Gel Filtration colum chromatography.(A) Column chromatography of Superdex 200 column as the final purification step. In all cases, 20 mM Tris-HCl buffer, pH 8.0 containing 0.3 M NaCl and 0.2% SB3-12 was used as the eluted buffer. (B) Calibration curve for the determination of molecular weight of the purified FDH_{S77} by gel filtratration using Superose 12 HR. The FDH_{S77} eluted at a position corresponding to 150 kDa. The column was calibrated with standard molecular weight markers (Bio-Rad Lab Laboratories Inc.): bovine thyroglobulin (M_r = 670,000), bovin γ-globulin (M_r = 158,000), chicken ovalbumin (M_r = 44,000), horse myoglobin (M_r = 44,000), vitamin B_{12} (M_r = 1350).

2.3.4. Kinetic properties

In the assay conditions of BV as an electron accepter, The purified FDH_{S77} showed a specific activity of 24.5 U/mg for the condition of 10 mM BV, which is almost 10-fold greater that that (2.4 U/mg) of FDH–N from *E. coli*.[9] In the steady-state, kinetic

parameters were determined by using the Michaelis-Menten equation at pH 7.0 and 30°C. The K_m value for formate of the FDH_{S77} was estimated to be 0.44 mM on the conditions of BV (10 mM) as an electron acceptor (Figure 2.8). This K_m value indicates that the FDH_{S77} shows substantially higher affinity for formate than other bacterial FDHs, such as the K_m values of *D. desulfurican* (21 mM) and *Clostridium pasteuriaum* (1.7 mM).[23,24] The limiting rate (V_{max}) was estimated as 30.4 U/mg (Figure 2.8). The turnover number (k_{cat}) was calculated as 76 s^{-1}, using the calculated FDH_{S77} molecular mass of 150 kDa. The specificity constant (k_{cat}/K_m) for formate was 1.73×10^5 $M^{-1}s^{-1}$.

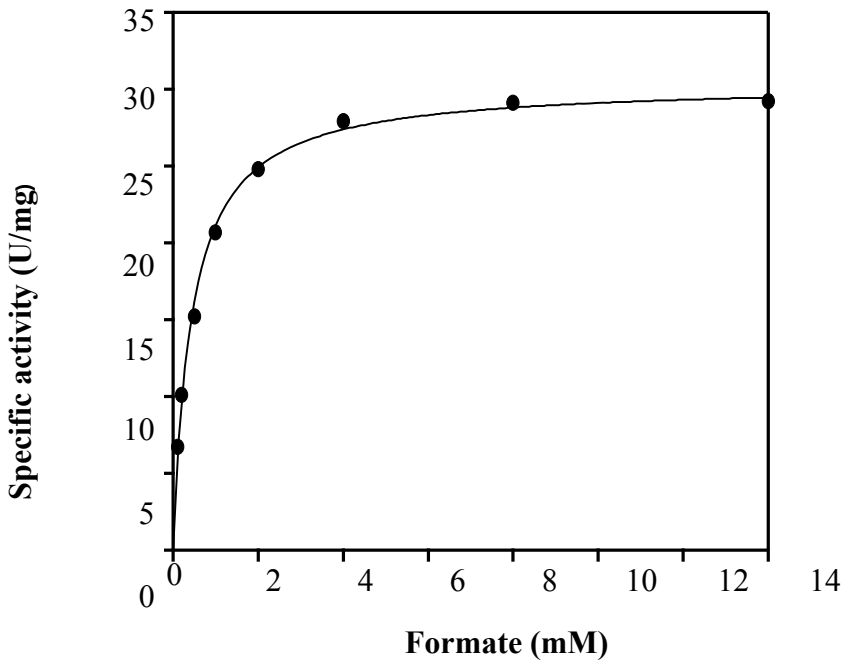

Figure 2.8 Steady-rate kinetic assays of the FDH_{S-77} for the reaction of formate-oxidation. BV was used as an electron acceptor. The concentration of sodium formate was varied from 0.1 to 15 mM. The assays were performed at 30°C, pH 7.0. The obtained data were fitted to the Michaelis-Menten equation using nonlinear regression.

2.3.5. Effects of pH and temperature on FDH activity

The FDH_{S77} has high thermostability and pH resistance. The optimal temperature for the FDH_{S77} activity was 80°C (Figure 2.9). The activity at 80°C was almost 5-fold higher than that at 30°C (24.5 U/mg), reaching 132.3 U/mg. Considering the growth temperature (32°C) of strain S-77, the FDH_{S77} displayed a high thermostability, indicating a half-life of activity of ca. 20 min at 70°C under anaerobic conditions. In addition, the purified FDH showed a high catalytic activity over a wide pH range. The maximal activity was observed at pH 8.5 (Figure 2.10), but the activity decreased at low pH. Although the optimum reaction of the FDH_{S77} was pH 8.5, the FDH_{S77} showed remarkable pH resistance even at significant acidic ranges below pH 4.0 (Figure 2.10). The FDH retained more than 70% of the initial activity, even after 3 h incubation at pH 3.0.

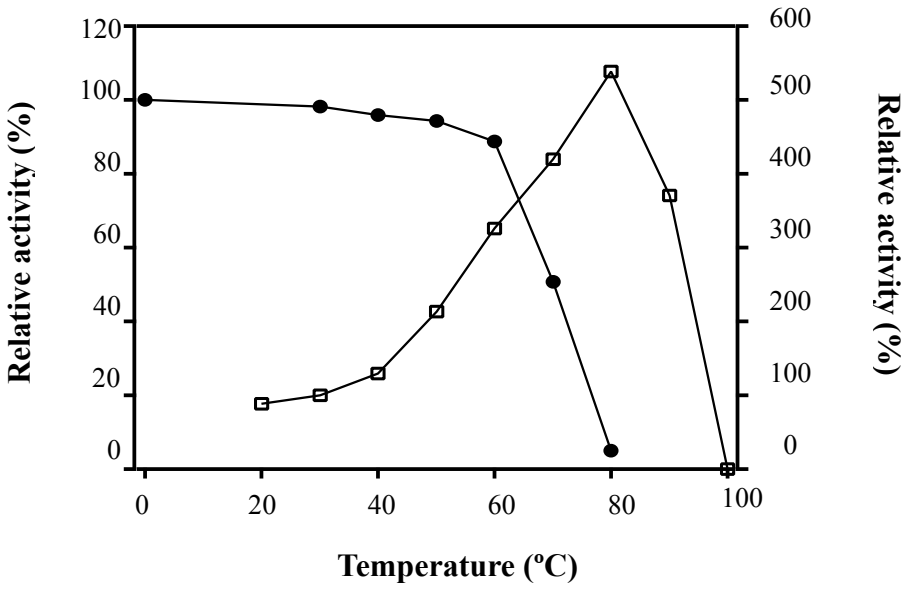

Figure 2.9 Effect of temperature on the activity of the purified FDH_{S77}. Thermostability of the purified FDH_{S77} after treatment for 20 min between 0°C and 80°C under N_2 (closed circles) and optimal reaction temperature of the FDH_{S77} (open squares). The

FDH activity was measured at pH 7.0. The obtained data were calculated by the means of at least three independent experiments.

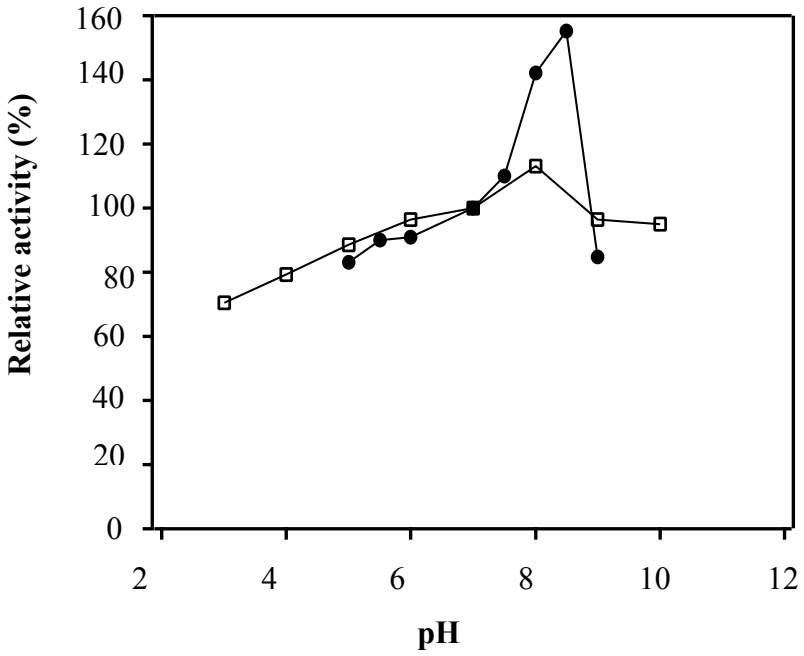

Figure 2.10 Effect of pH value for the activity of the purified FDH_{S77}: pH stability of the purified FDH_{S77} after treatment for 3 h at 4°C between pH 3.0 and 10.0 under N_2 gas (open squares) and the optimum reaction pH of the purified FDH_{S77} (closed circles). The obtained data were calculated by the means of at least three independent experiments.

2.3.6. Stability of the FDH_{S77} in air

The anaerobically purified FDH_{S77} could immediately reduce BV upon direct injection into a reaction mixture under anaerobic conditions. Surprisingly, the oxidized FDH_{S77}, even after the enzyme is exposed to air for 6 h at 4°C, can be restored up to 80% of its original specific activity (Figure 2.11). However, the activity was not

completely recovered. The oxidized enzyme required lag times (ca. 17 min) for its full reactivation (Figure 2.12). The specific activity after the end of the lag time, as shown in Figure 2.12-II, was almost the same as that of the anaerobically purified enzyme of Figure 2.12-I. In general, O_2-sensitive FDH shows a significant decline of specific activity, and easily loses catalytic ability after air oxidation.[9,10] Compared to other bacterial FDHs, the FDH_{S77} has a remarkable O_2-stability. O_2-stable FDHs were also reported from other microorganisms, such as those of *D. gigas,*[11,14] *D. desulfurican*,[23] *D. alsaskensis*,[25] *Rhodobacter capsulatus*,[26] and *E. coli*,[27] however, the mechanism for how to stabilize the aerobic conditions of the O_2-stable FDHs is not yet understood.

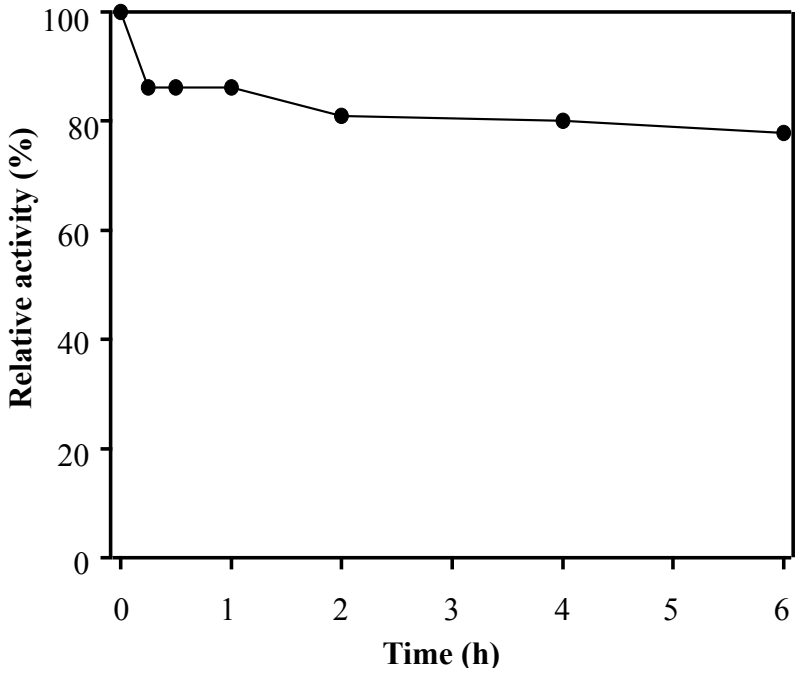

Figure 2.11 Long-term O_2-stability of the FDH_{S77}. The purified FDH_{S77} was exposure to an air, then incubated at 4°C. The remaining activities were measured periodically during the air oxidation procedure. All reactions were started with injection of the oxidized enzyme directly into the anaerobic reaction solutions. All assays were carried out under the same buffer conditions of 50 mM MOPS buffer at pH 7.0 and at 30°C.

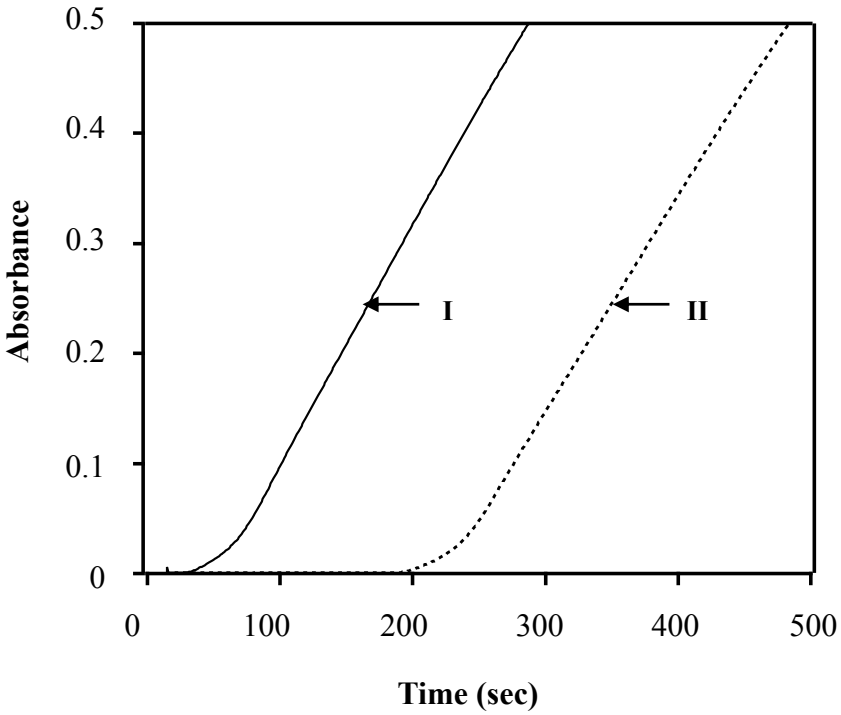

Figure 2.12 The effect of O_2 on the formate-oxidation of the purified FDH_{S-77}. Stability of the FDH_{S77} in air was determined by measuring the remaining activity after exposure to an air atmosphere. Requirement incubation time to recover activity of enzyme at initial time (solid line); and incubated in air for 1h at 4°C (dotted line).

2.3.7. Electrochemical experiments of the FDH_{S77}

We have investigated the stability of purified FDH_{S77} in air was also determined by the amperometric method. Amperometric detection of the FDH_{S77} was first held under a headgas of 100% N_2 at a reference potential of -200 mV vs. Ag/AgCl electrode. The FDH_{S77} generated an extremely stable electric current of formate-oxidation at the conditions (Figure 2.13). Surprisingly, the reduced current was recovered by continuous bubbling of N_2 to flush out the dissolved O_2 into the reaction solution. As shown in Figure 2.13, reactivation of the enzyme occurred within 300 s. However, the current density drastically decreased toward zero when the flowing gas in the electrochemical

cell was changed from N_2 to air. After substantial reduction, the current density for formate oxidation could be restored to near its initial current density after of approximately 1000 s. This intriguing result suggests that the FDH_{S77} has an excellent stability against O_2.

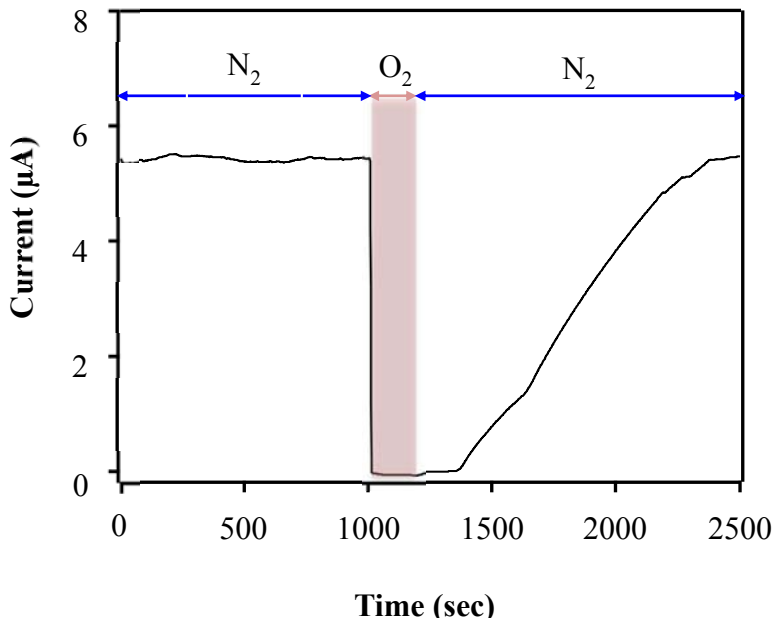

Figure 2.13 Amperometric *i-t* curve of FDH_{S77}. In the initial reaction 100% N_2 was bubbled into the reaction solution. After recording the catalytic current of formate-oxidation for 1000 s, 100 % O_2 was bubbled into the solution for 90 s. Subsequently, the bubbling gas was change from O_2 to N_2 to flush out the dissolved O_2 into the solution. Experimental data was recorded under the conditions with a potential at -200 mV vs. SHE with rotating the working electrode at 3000 rpm using a gas flow rate of 1000 scc/min.

2.3.8. UV-visible spectra of the purified FDH_{S77}

The UV/visible spectra of air-oxidized FDH_{S77} exhibited a broad absorption peak around 400 nm and a slight shoulder in the 310 nm region (Figure 2.14), which is a typical feature of non-heme containing iron proteins.[20,28] The result suggests that the purified FDH_{S77} did not contain *b*-type heme, which exhibited no typical α-absorption peak of the reduced state around 560 nm. However, absorbance in this region around 400 nm decreased by reduction of sodium dithionite under anaerobic conditions.

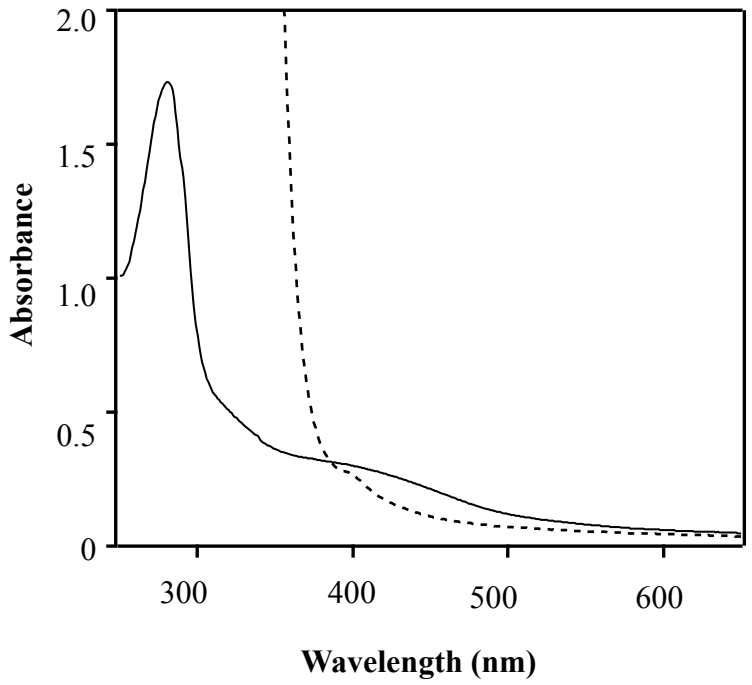

Figure 2.14 UV-visible absorption spectra of the purified FDH_{S77} (1.75 mg/ml) in 50mM K-phosphate buffer, pH 1.0, containing 0.1 M NaCl and 0.2% SB3-12. Solid line: the air oxidizied FDH_{S77}. Dotted line: the reduced FDH_{S77} by addition of sodium dithionite.

2.3.9. EPR Spectra and ICP-MS analysis of the purified FDH_{S77}

The result of ICP-MS analysis indicates that the purified FDH_{S77} contains molybdenum (0.97 atom/molecule), selenium (1.2 atom/molecule), and iron (17.5 atoms/molecule), but not tungsten. Together with the iron content, the FDH_{S77} may possess five [4Fe-4S] clusters; whereas FDH-N from *E. coli* contains five [4Fe-4S] clusters[13] and FDH from *D. gigas* contains four [4Fe-4S] clusters.[14] The amount of iron content suggests that the purified FDH_{S77} may be slightly damaged by some degradation of iron sulfur clusters during the procedures of solubilization and purification.

In addition, the oxidized FDH_{S77} was EPR silent, suggesting that the active center of the enzyme was the Mo(VI) state. The formate-reduced FDH_{S77} exhibited the rhombic EPR spectrum at g = 2.018, 1.994, and 1.961 at 110 K (Figure 2.15). The signal is attributed to the representative signals from Mo(V) of FDH.[29,30] The Mo(V) EPR signals of formate-reduced FDHs from *D. desulfuricans* were detected at g-values of 2.012, 1.996, and 1.985 and that of *Methylobacterium* sp. RXM was observed at 2.002, 1.987, and 1.959. The signal intensity increases with increasing microwave power. Although the line shape of the EPR spectra of FDH_{S77} was not completely identical to those of other FDHs, the EPR signal apparently arose from the Mo(V) state.[29.30] On the basis of the results of ICP-MS analysis and EPR spectra, the purified FDH_{S77} belongs to the family of Mo containing FDH.

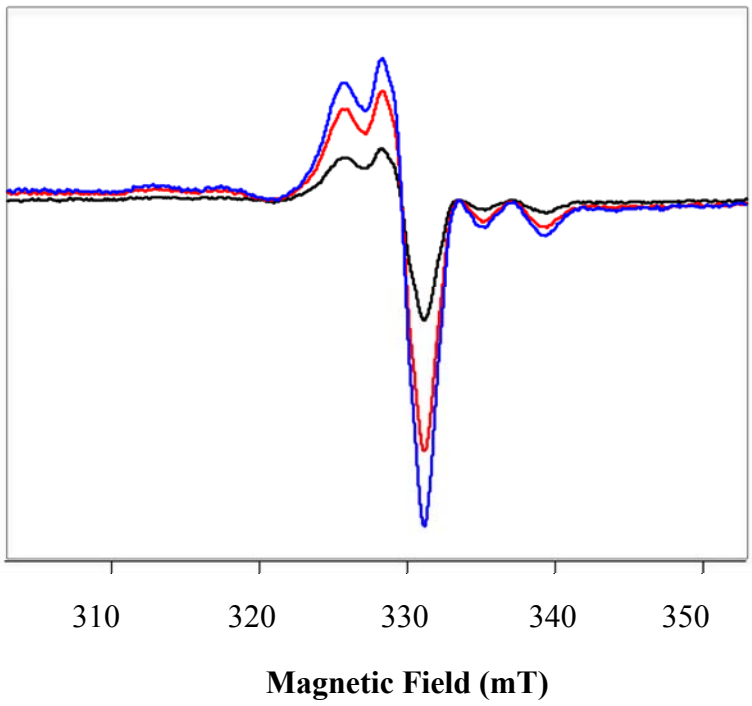

Figure 2.15 EPR spectra of formate-reduced FDH_{S77}. The EPR experiments were carried out using freshly purified FDH_{S77} (10 mg/mL) equilibrated with 10 mM Tris-HCl buffer, pH 8.0, containing 0.1 M NaCl and 0.2% SB3-12. FDH_{S77} was reduced by addition of 10 mM formate into the enzyme solution and then incubated for 20 min at 30°C under anaerobic conditions. Experimental conditions: 1 mW (black line), 5 mW (red line) and 10 mW (blue line) microwave power; 80 mT modulation amplitude; 9.20 GHz microwave frequency.

2.4. DISCUSSION

In order to discover robust formate dehydrogenase from nature, we have the plan to isolate new bacteria from extreme environments, such as various springs in the Kyushu area, Japan. In the same time, we have also retrieved useful genomic information from the databases of the National Center for Biotechnology Information. We have eventually isolated a novel bacterium, *Citrobacter* sp. S-77 from the water samples of a tepid spring at Aso-Kuju National Park, Kumamoto.[16] In the previously studies, we have purified and characterized a novel membrane-bound [NiFe]hydrogenase (MBH) from the same bacterium.[16] The MBH shows a remarkably O_2-stability and high H_2-activation, which has a great potential for use as a biocatalyst in industrial applications. In fact, the high active and O_2-stable membrane-bound [NiFe]hydrogenase (MBH) plays an anode electron as an extraordinary activity for H_2-oxidation in polymer electrolyte fuel cell.[17] At this time, we have found an O_2-stable formate dehydrogenase from our newly isolated microorganisms. Among several isolated strains, I can detect highly active and O_2-stable FDH activity in the isolated membrane fraction. The strain S-77 belongs to *Citrobacter* species, which is a facultative anaerobic bacterium, which can grow well under aerobic and anaerobic growth conditions around 32°C.[16] *Citrobacter* sp. S-77 belongs to the family of *Enterobacteriaceae*, suggesting that the FDH_{S77} may have similar characteristics to those of the FDH-N from *E. coli*. The purified FDH from membrane fraction was a molecular weight of 150 kDa that is a significantly different to 510 kDa of the FDH-N from *E. coli*. The FDH-N is composed of a trimer of heterotetramers.[8,9,11] However, the purified FDH_{S77} consisted of two subunits of approximately 95 kDa for the large subunit and 32 kDa for the small subunit (Figure 2.2), which is very similar to those of the periplasm-localized FDHs from *D.*

gigas and *D. desulfurican*.[14,23] As the results of all the FDHs reported so far, the heterodimeric structure of the FDH is considered to be biologically relevant. According to the N-terminal amino acid sequence analysis, the FDH_{S77} is highly homologous to the FDH-N from *E. coli*. In comparison to the amino acid sequences of other bacterial FDHs (www.ncbi.nlm.nih.gov), we have found that the initial 33 amino acid residues of large subunit of FDHs contains the signal sequence of a twin-arginine translocase (Tat) motif RRXFK (Figure 2.5).[31] The N-terminal sequence determined for the large subunit of the purified FDH_{S77} begins after the Tat signal peptide. Metalloenzyme complexes of FDH is exported from cytoplasm to periplasm portion by a Tat pathway,[31,27] where the Tat signal sequence of the large subunit plays an important role in FDH secretion from cytoplasm to periplasm portion across the membrane.

On the other hand, the O_2-tolerant MBH has contains the Tat system, which serves in the translocation of MBH. In the MBH, the Tat signal sequence contains in a small subunit of MBH, whereas the large subunit lacks the targeting signal sequence.[33] Membrane-anchoring proteins are commonly cleaved at the boundary surface of the inner membrane or transmembrane helix when the steps of solubilization and purification are performed. The exquisite example is the O_2-tolerant MBH-cytochrome *b* complex.[16,20,29,30] The cytochrome *b* subunit of MBH and a C-terminal transmembrane helice in the small subunit were spontaneously cleaved off during solubilization and purification processes. Based on the current results, we predict that the transmembrane portion of the small subunit and the inner membrane protein of the cytochrome *b* subunit of the purified FDH_{S77} also appear to be cleaved from the FDH complex during some purification steps. This might also affect the degradation or cleavage of the 95 kDa large subunit, which results in the production of the 87 kDa

protein fragment observed on SDS-PAGE analysis. However, the cytochrome *b* subunit is an *in vivo* essential part of the FDH complex as an electron acceptor, which functions as an electron transfer chain.[14,31] In *Citrobacter* sp. S-77, the O_2-stable FDH_{S77} may have an important role in the membrane-associated electron transport chain. The O_2-stable FDH may have structural features to function efficiently under an aerobic environment. Although there is currently no defined structural information on the O_2-stable FDH_{S77}, we predict that the difference in amino acid environment in the catalytic center or electron transfer iron-sulfur clusters may be involved in the O_2-stability of the enzyme.

2.5. CONCLUSIONS

In this research, I purified and characterized a new membrane-bound formate dehydrogenase from a newly isolated bacterium *Citrobacter* sp. S-77. We determined the N-terminal amino acid sequences of the purified FDH_{S77} and the draft genome sequence of the strain S-77. The assigned the gene encoding of FDH_{S77} indicated that the FDH_{S77} is analogous to FDH-N from *E. coli*. Apart from the scientific interest in the physiological role of the O_2-stable FDH along with its thermostability and pH resistance, the FDH_{S77} is also of interest in the application perspective. The prominent stability of the FDH_{S77} is more likely to accelerate our interest in determining further biochemical and structure-functional studies that will lead to a better understanding of the molecular mechanism of formate-oxidation of the O_2-stable FDH.

REFERENCES

1. **Berg, I. A.**: Ecological aspects of the distribution of different autotrophic CO_2 fixation pathways, Appl. Environ. Microbiol., **77**, 1925-1936 (2011).
2. **Appel, A. M., Bercaw, J. E., Borcarsly, A. B., Dobbek, H., DuBois, D. L., Dupuis, M., Ferry, J. G., Fujita, E., Hille, R., Kenis, P. J. A., and other 10 authors**: Frontiers, opportunities, and challenges in biochemical and chemical catalysis of CO_2 fixation, Chem. Rev., **113**, 6621-6658 (2013).
3. **Ihara, M., Kawano, Y., Urano, M., and Okabe, A.**: Light driven CO_2 fixation by using cyanobacterial photosystem I and NADPH-dependent formate dehydrogenase, PLoS One., **8**, e71581 (2013).
4. **Ferry, J. G.**: Formate dehydrogenase, FEMS Microbiol. Rev., **87**, 377-382 (1990).
5. **Gonzalez, P. J., Rivas, M. G., Mota, C. S., Brondino, D. C., Moura, I., and Moura, J. J. G.**: Periplasmic nitrate reductases and formate dehydrogenases: biological control of the chemical properties of Mo and W for fine tuning of reactivity, substrate specificity and metabolic role, Coord. Chem. Rev., **257**, 315-331 (2013).
6. **Tishkov, V. I. and Popov, V. O.**: Protein engineering of formate dehydrogenase, Biomol. Eng., **23**, 89-110 (2006).
7. **Yu, X. and Pickup, P. G.**: Recent advances in direct formic acid fuel cells (DFAFC), J. Power Sources, **182**, 124-132 (2008).
8. **Sawers, G.**: The hydrogenases and formate dehydrogenase of *Escherichia coli*, Antonie van Leeuwenhoek, **66**, 57-88 (1994).

9. **Enroch, H. G. and Lester, R. L.**: The purification and properties of formate dehydrogenase and nitrate reductase from *Escherichia coli*, J. Biol. Chem., **250**, 6693-6705 (1975).

10. **Axley, M. J., Grahame, D. A., and Stadtman, T. C.**: *Escherichia coli* formate-hydrogenase lyase. Purification and properties of the selenium-dependent formate dehydrogenase component, J. Biol. Chem., **265**, 18213-18218 (1990).

11. **Almendra, M. J., Brondino, C. D., Gavel, O., Pereira, A. S., Tavares, P., Bursakov, S., Duarte, R., Caldeira, J., Moura, J. J., and Moura, I**.: Purification and characterization of a tungsten-containing formate dehydrogenase from *Desulfovibrio gigas*, Biochem., **38**, 16366-16372 (1999).

12. **Boyington, J. C, Gladyshev, V. N., Khangulov, S. V., Stadtman, T. C., and Sun, P. D.**: Crystal structure of formate dehydrogenase H: catalysis involving Mo, molybdopterin, selenocysteine, and a Fe_4S_4 cluster, Science, **275**, 1305-1308 (1997).

13. **Jormakka, M., Törnroth, S., Byrne, B., and Iwata, S.**: Molecular basis of proton motive force generation: structure of formate dehydrogenase-N, Science, **295**, 1863-1868, (2002).

14. **Raaijmakers, H., Macieira, S., Dias, J. M., Teixeira, S., Bursakov, S., Huber, R., Moura, J. J., Moura, I., and Romão, M. J.**: Gene sequence and the 1.8 Å crystal structure of the tungsten-containing formate dehydrogenase from *Desulfovibrio gigas*, Structure, **10**, 1261-1272 (2002).

15. **Sawers, R. G**.: Formate and its role in hydrogen production in *Escherichia coli*, Biochem. Soc. Trans., **33** (2005).

16. **Eguchi, S., Yoon, K.-S., and Ogo, S.**: O_2-stable membrane-bound [NiFe]hydrogenase from a newly isolated *Citrobacter* sp. S-77, J. Biosi. Bioeng., **114**, 479-484 (2012).
17. **Matsumoto, T., Eguchi, S., Nakai, H., Hibino, T., Yoon, K.-S., and Ogo, S.**: [NiFe]Hydrogenase from *Citrobacter* sp. S-77 surpasses platinum as an electrode for oxidation reaction, Agrew. Chem. Int. Ed., **53**, 8895-8898 (2014).
18. **Kim, S., Seol, E., Raj, S. M., Park, S., Oh, Y.-K., and Ryu, D. D. Y.**: Various hydrogenases and formate-dependent hydrogen production in *Citrobacter amalonaticus* Y19, Int. J. Hydrogen Energy, **33**, 1509-1515 (2008).
19. **Zatsepin, S. S. and Netrusov, A. I.**: Enzyme activity of the formate hydrogenlyase complex in *Citrobacter freundii*, Mikrobiologiia, **53**, 246-250 (1984).
20. **Yoon, K.-S., Fukuda, K., Fujisawa, K., and Nishihara, H.**: Purification and characterization of a highly thermostable, oxygen-resistant, respiratory [NiFe]-hydrogenase from a marine, aerobic hydrogen-oxidizing bacterium *Hydrogenovibrio marinus*, Int. J. Hydrogen Energy, **36**, 7081-7088 (2011).
21. **Matsudaira, P.**: Sequence from picomole quantities of proteins electroblotted onto polyvinylidene difluoride membranes, J. Biol. Chem., **262**, 10035-10038 (1987).
22. **Lowry, O. H., Rosebrough, N. J., Farr, A. L., and Randall, R. J.**: Protein measurement with the folin phenol reagent, J. Biol. Chem., **193**, 265-275 (1951).
23. **Costa, C., Teixeira, M., LeGall, J., Moura, J. J. G., and Moura, I.**: Formate dehydrogenase from *Desulfovibrio desulfuricans* ATCC 27774: isolation and spectroscopic characterization of the active sites (heme, iron-sulfur centers and molybdenum), J. Biol. Inorg. Chem., **2**, 198-208 (1997).

24. **Liu, C.-L. and Mortenson, L. E.**: Formate dehydrogenase of *Clostridium pasteurianum*, J. Bacteriol., **159**, 375-380 (1984).

25. **Brondino, C. D., Passeggi, M. C. G., Caldeira, J., Almendra, M. J., Feio, M. J., Moura, J. J. G., and Moura, I.**: Incorporation of either molybdenum or tungsten into formate dehydrogenase from *Desulfovibrio alaskensis* NCIMB 13491; EPR assignment of the proximal iron-sulfur cluster to the pterin cofactor in formate dehydrogenases from sulfate-reducing bacteria, J. Biol. Inorg. Chem., **9**, 145-151 (2004).

26. **Hartmann, T. and Leimkühler, S.**: The oxygen-tolerant and NAD^+-dependent formate dehydrogenase from *Rhodobacter capsulatus* is able to catalyze the reduction of CO_2 to formate, FEBS J., **280**, 6083-6096 (2013).

27. **Sousa, P. M., Videira, M. A., and Melo, A. M.**: The formate:oxygen oxidoreductase supercomplex of *Escherichia coli* aerobic respiratory chain, FEBS Lett., **587**, 2559-2564 (2013).

28. **Mota, C. S., Valette, O., González, P. J., Brondino, C. D., Moura, J. J. G., Moura, I., Dolla, A., and Rivas, M. G.:** Effects of molybdate and tungstate on expression levels and biochemical characteristics of formate dehydrogenases produced by *Desulfovibrio alaskensis* NCIMB 13491, J. Bacteriol., **193**, 2917-2923 (2011).

29. **Rivas, M. G., González, P. J., Brondino, C. D., Moura, J. J. G., and Moura, I.:** EPR characterization of the molybdenum(V) forms of formate dehydrogenase from *Desulfovibrio desulfuricans* ATCC 27774 upon formate reduction, J. Inorg. Biochem., **101**, 1617-1622 (2007).

30. **Duarte, R. O., Reis, A. R., Gírio, F., Moura, I., Moura, J. J. G., and Collaço, T. A.**: The formate dehydrogenase isolated from the aerobe *Methylobacterium* sp. RXM is a molybdenum-containing protein, Biochem. Biophys. Res. Commun., **230**, 30-34 (1997).

31. **Jormakka, M., Byrne, B., and Iwata, S.**: Formate dehydrogenase – a versatile enzyme in changing environments, Curr. Opin. Struct. Biol., **13**, 418-423 (2003).

32. **Sargent, F., Berks, B. C., and Palmer, T.**: Assembly of membrane-bound respiratory complexes by the Tat protein-transport system, Arch. Microbiol., **178**, 77-84 (2002).

33. **Wu, L.-F., Chanal, A., and Rodrigue, A.**: Membrane targeting and translocation of bacterial hydrogenases, Arch. Microbiol. **173**, 319-324 (2000).

34. **Fritsch, J., Lenz, O., and Friedrich, B.**: The maturation factors HoxR and HoxT contribute to oxygen tolerance of membrane-bound [NiFe] hydrogenase in *Ralstonia eutropha* H16, J. Bacteriol., **193**, 2487-2497 (2011).

35. **Shomura, Y., Yoon, K.-S., Nishihara, H., and Higuchi, Y.**: Structural basis for a [4Fe-3S] cluster in the oxygen-tolerant membrane-bound [NiFe]-hydrogenase, Nature, **479**, 253-256 (2011).

CHAPTER 3

A [NIFE]HYDROGENASE MODEL THAT CATLYSES THE RELEASE OF HYDROGEN FROM FORMIC ACID

ABSTRACT

In Chapter 3, I report the decomposition of formic acid to hydrogen and carbon dioxide, catalyzed by a (μ-hydrido)(formato) $Ni^{II}Ru^{II}$ complex, [Ni^{II}L(μ-H)(HCOO)Ru^{II}(η^6-C_6Me_6)], L = *N*,*N*'-dimethyl-3,7-diazanonane-1,9-dithiolato), which is developed from a [NiFe]hydrogenase model. This is the first example of H_2 evolution, catalyzed by a [NiFe]hydrogenase model without additional energy. The structure of (μ-hydrido)(formato) $Ni^{II}Ru^{II}$ complex was characterized by X-ray analysis, electrospray ionization mass spectrometry (ESI-MS), UV-vis spectroscopy, and IR spectroscopy. X-ray crystallographic analysis of the (μ-hydrido)(formato) $Ni^{II}Ru^{II}$ complex reveals a NiS_2Ru butterfly core with a bridging hydride. The turnover numbers of H_2 evolution that is catalyzed by the (μ-hydrido)(formato) $Ni^{II}Ru^{II}$ complex is 857 for 1 h at pH 3.5.

3.1. INTRODUCTION

Hydrogen is promised candidate for our future energy system. H_2 is a clean energy, because it is combusted in engines of fuel cells, only water emerges as benign exhaust. However, it requires either high cost for storage and transportation of H_2.[1-3] In contrast to these materials, formic acid has been good candidate of H_2 carrier.[4-6] Therefore, the H_2 evolution from the decomposition of formic acid has been recently investigated.

In biological energy system, formate hydrogenlyase (FHL) is an enzyme complex that is responsible for conversion of formic acid into the gaseous products CO_2 and H_2 (equation 3.1).[7-9] The FHL consisted of formate dehydrogenase-H (FDH-H),[10-12] which catalyzes extraction of protons and electrons from HCOOH (equation 3.2), and a [NiFe]hydrogenase ([NiFe]H_2ase), which is recombines those protons and electrons into H_2 (equation 3.3).[13-23] Thus, the FHL plays an important role in natural organism and are attracted model for development a effective catalyst of H_2 evolution.

$$HCOOH \xrightleftharpoons{FHL} CO_2 + H_2 \qquad (3.1)$$

$$HCOOH \xrightleftharpoons{FDH} CO_2 + 2H^+ + 2e^- \qquad (3.2)$$

$$2H^+ + 2e^- \xrightleftharpoons{[NiFe]H_2ase} H_2 \qquad (3.3)$$

The FHL comprises seven proteins of HycB, HycC, HycD, HycF, and HycG and with components of formate dehydrogenase H (FDH-H) with hydrogenase 3 (HycE).[7-9] With the exception of FDH-H, the other six components are all encoded in a single *hyc* operon (Figure 3.1).[7]

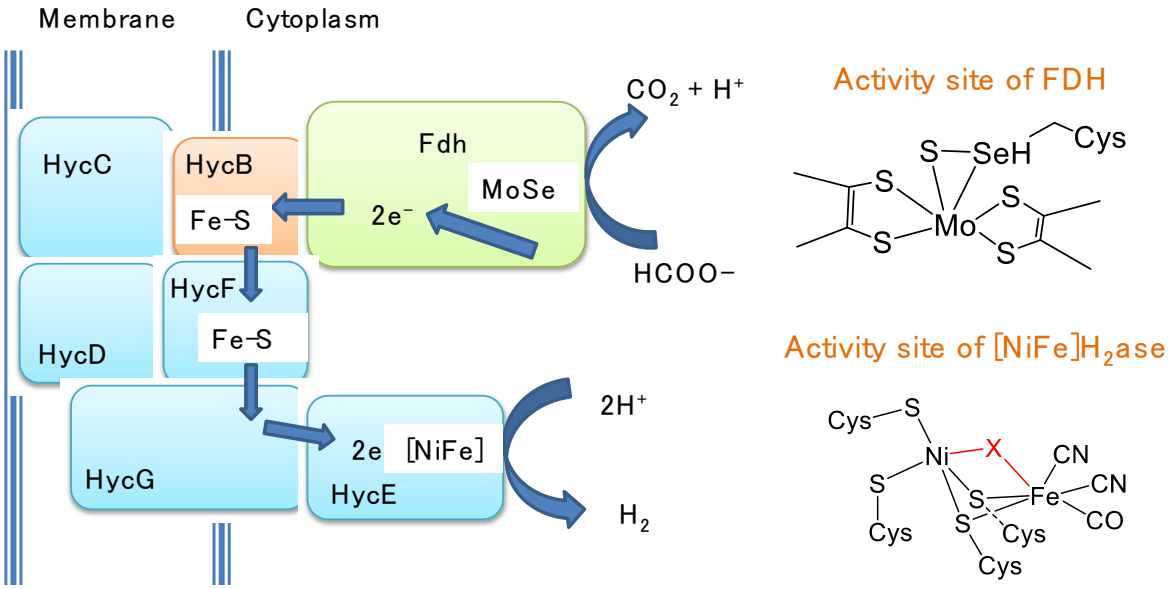

Figure 3.1 The structure of FHL enzyme complex (adapted from ref. 7). The FHL comprises seven proteins of HycB, HycC, HycD, HycF, HycG, FDH-H (Fdh), and hydrogenase 3 (HycE).

The crystal structure of FDH-H from *E. coli* was determined to reveal that the enzyme has a four-domain structure with the molybdenum coordinated by selenium and both MGD cofactors.[24] The components of FDH-H and HycE are cytoplasmic located proteins, but the components of HycB, HycC, HycD, HycF, and HycG are integral membrane proteins.

Model studies of [NiFe]H_2ase with regard to H_2 evolution have been reported so far. Most of complexes have to need additional energy. For example, a NiFe catalyst, reported by Rauchfuss et al., that requires additional electrical energy[25] and a $NiFe_2$ catalyst, reported by Schröder et al., that requires additional light energy[26] have been published. Thus, a biomimetic catalyst as a model for [NiFe]H_2ase for H_2 production capable of working at ambient temperature and pressure has certainly been desired.

A dinuclear Ni(μ-H)Ru complex $[Ni^{II}L(H_2O)(\mu\text{-}H)Ru^{II}(\eta^6\text{-}C_6Me_6)](NO_3)$ {[**2**](NO_3)}, where L = *N*,*N*'-dimethyl-3,7-diazanonane-1,9-dithiolato,[27] has been synthesized from the reaction of a dinuclear NiRu aqua complex $[Ni^{II}LRu^{II}(H_2O)(\eta^6\text{-}C_6Me_6)][(NO_3)_2$ {[**3**]$(NO_3)_2$} with H_2 in water under ambient conditions (20°C and 0.1 MPa). The Ni(μ-H)Ru complex **2** is close to the active site structure of [NiFe]H_2ase. Since we have developed a successful [NiFe]H_2ase model catalyst, we felt that it would be a good candidate for a FHL model system, which proved to be the case.[29-31]

Here, we report the first example of a [NiFe]H_2ase model catalyst that is capable both of heterolytically spitting hydrogen gas into protons and electrons and of decomposing formic acid into CO_2 and H_2 without additional energy.

3.2. EXPERIMENTAL METHODS

3.2.1. Material and methods

All experiments were carried out under an N_2 or Ar atmosphere by using standard Schlenk techniques and glovebox. H_2 gas (99.9999%) was purchased from Taiyo Sanso Co., Ltd. Concentrated HNO_3/H_2O, distilled water and HCOONa were purchased from

Wako Pure Chemical Industries, Ltd. Concentrated DNO_3/D_2O (99% D), 40wt% $NaOD/D_2O$ (99% D), DCOONa and D_2O (99% D) were purchased from Cambridge Isotope Laboratores, Inc. $[Ni^{II}L(H_2O)(\mu\text{-}H)Ru^{II}(\eta^6\text{-}C_6Me_6)](NO_3)$ {[**2**](NO_3), L = *N*,*N*'-dimethyl-3,7-diazanonane-1,9-dithiolato} and $[Ni^{II}L(H_2O)(\mu\text{-}H)Ru^{II}(\eta^6\text{-}C_6Me_6)](NO_3)_2$ were prepared by the methods described in the literature.[27]

pH (pD) values of the aqueous solutions were determined by a pH meter (TOA, HM20J) equipped with a pH combination electrode (TOA, GST-5725C). Values of pD were corrected by adding 0.4 to the observes values (pD = pH meter reading + 0.4). The pH (or pD) of aqueous solutions were adjusted by concentrated HNO_3/H_2O (or DNO_3) and 10 M $NaOH/H_2O$ ($NaOD/D_2O$) and 10 M $NaOH/H_2O$ ($NaOD/D_2O$).[32,33]

Electrospray ionization mass spectrometry (ESI-MS) data were obtained by a JEOL JMS-T100LC AccTOF. IR spectra of solid compounds in KBr disks were recorded on a Thermo Nicolet NEXUS 8700 FT-IR instrument from 650 to 4500 cm^{-1} using 2 cm^{-1} standard resolution at 25°C (light pass length: 0.10 cm). Elemental analysis data was obtained by a Perlin Elmer 2400II series CHNS/O analyzer. H_2 gas was determined by a Shimadzu GC-14B and GC-8A gas chromatograph {He carrier, 10% $MnCl_2$-alumina column (model: Shinwa OGO-SP) at -196°C (liquid N_2)}. CO_2 gas was determined by a Shimadzu GC-2014 chromatograph.

3.2.2. Synthesis of $[Ni^{II}L(HCOO)(\mu\text{-}H)Ru^{II}(\eta^6\text{-}C_6Me_6)]$ (1).

Complex **1** is able to be synthesized from complex [**2**](NO_3) (method A) and complex [**3**]$(NO_3)_2$ (method B) as starting materials as follows.

Method A. An aqueous solution (2.0 mL) of [**2**](NO_3) (50.1 mg 0.0804 mmol) was added to an aqueous solution (2.0 mL) of HCOONa (0.547 g, 8.04 mmol) at 25°C. The resulting solution was allowed to stand overnight to gradually precipitated brown crystals, which were collected by filtration and dried in vacuo {yield: 73% based on [**2**](NO_3)}.

Method B. An aqueous solution (5.0 mL) of HCOONa (1.54 g, 22,7 mmol) was added to an aqueous solution (5.0 mL) of [**3**](NO_3)$_2$ (152 mg, 0.222 mmol) at 25°C. The resulting solution was allowed to stand for 4 h to gradually precipitate brown crystals, which were collected by filtration and dried *in vacuo* brown crystals, which were collected by filtration and dried in vacuo {yield: 34% base on [**3**](NO_3)$_2$}. Positive-ion ESI-MS (in H_2O at pH 7.0): *m/z* 543.2 {[**1**−HCOO]$^+$, relative intensity (I) = 100% in the range of *m/z* 633.2 ([**1** + HCOO]$^-$, *I* = 100% in the range of *m/z* 200-2000). FT-IR (cm^{-1}, KBr disk); 1349, 1760, 2649. Anal. Calcd for [**1**]·2H_2O:$C_{22}H_{44}N_2NiO_4RuS_2$: C, 42.31; H, 7.1; N, 4.49. Found: C, 42,34; H, 7.0; N, 4.39.

3.2.3. Synthesis of [Ni^{II}L(DCOO)(μ−D)Ru^{II}(η^6−C_6Me_6)] (double D-labelled 1).

A solution of DCOONa (151 mg, 2.19 mmol) in D_2O (0.5 mL) at 25°C. The resulting solution was allowed to stand for 4 h to gradually precipitate brown crystals, which were collected by filtration and dried in vacuo {yield: 34% based on [**3**](NO_3)$_2$}. Positive-ion ESI-MS (in D_2O at pD 7.0): *m/z* 544.2 ([**1**−DCOO]$^+$, *I* = 100% in the range of *m/z* 200-2000). Negative-ion ESI-MS (in D_2O at pH 7.0): *m/z* 636.3 ([double D-labelled **1** + DCOO]$^+$, *I* = 100% in the range of m/z 200-2000). FT-IR (cm^{-1}, KBr disk): 1248, 1329, 2114.

3.2.4. Typical procedure for H_2 and CO_2 evolution from HCOOH catalyzed by $[Ni^{II}L(H_2O)(\mu\text{-}H)Ru^{II}(\eta^6\text{-}C_6Me_6)]$

A 3 mL vial was charged with 7.3 nmol of [**2**](NO_3) and 146 μmol of HCOONa in H_2O (500 μL) at pH 1.6 − 9.0, was capped with a septum under N_2 atmosphere. The vial was heated at 60°C for 1 h. The gas present in the vial was sampled using a gas-tight syringe and was analyzed for H_2 and CO_2 gases by GC.

3.2.5. X-ray crystallographic analysis.

A brown crystal of **1** used for X-ray analysis was obtained from its aqueous solution. Crystallographic data for **1**·5H_2O has been deposited with a Cambridge Crystallographic Data Center as Supplementary Publication No. CCDC 1016741. Copies of the data can be obtained free of charge on application to CCDC, 12 Union Road, Cambridge CB1EZ, UK {Fax: (+44)1223-336-063; e-mail: deposit@ccdc.cam.ac.uk}. Measurements were made on a Rigaku/MSC Sturn CCD diffractometer with confocal monochromated MoKα radiation (λ = 0.7107 Å). Data collected and processed using the CrystalClear program (Rigaku). All calculations were performed using the CrystalStructure crystallographic software package except for refinement, which was performed using SHELXL-97.

Although five O atoms (O3, O4, O5, O6, and O7) are assigned as waters, the electron densities of H atoms binding to the O atoms are not found. Thus, refinement was carried out without these H atoms and the calculated molecular is different from the reported molecular weight. The short distances between O atoms (O3, O4, O5, O6 and O7) should be caused by hydrogen bonds.

3.3. RESULTS AND DISCUSSION

3.3.1. Synthesis and characterization of (μ-hydrido)(formato) $Ni^{II}Ru^{II}$ complex 1

The water-soluble (μ-hydrido)(formato) $Ni^{II}Ru^{II}$ complex, $[Ni^{II}L(HCOO)(\mu\text{-}H)Ru^{II}(\eta^6\text{-}Me_6Me_6)]$ (**1**), was synthesized by the reaction of the μ-hydrido $Ni^{II}Ru^{II}$ complex, $[Ni^{II}L(H_2O)(\mu\text{-}H)Ru^{II}(\eta^6\text{-}C_6Me_6)](NO_3)$ {[**2**](NO3)}, with one equivalent of HCOONa (equation 3.4), or by the reaction of the aqua $Ni^{II}Ru^{II}$ complex, {[**3**](NO3)2}, with two equivalents of HCOONa in water.

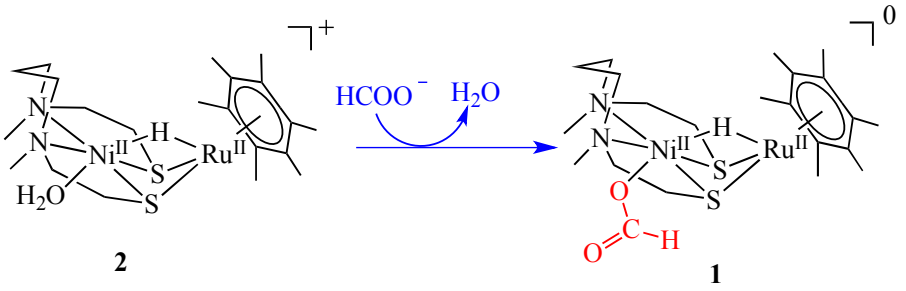

(Eq. 3.4)

Figure 3.2 shows the change of UV-vis spectra from [**2**](NO3) to **1**. One equivalent of HCOONa (2.34 μmol) was added into [**2**](NO3) (2.34 μmol) in H2O (2.0 mL). In the region between 250 and 370 nm, spectrum of **2** is shifted to spectrum of **1**.

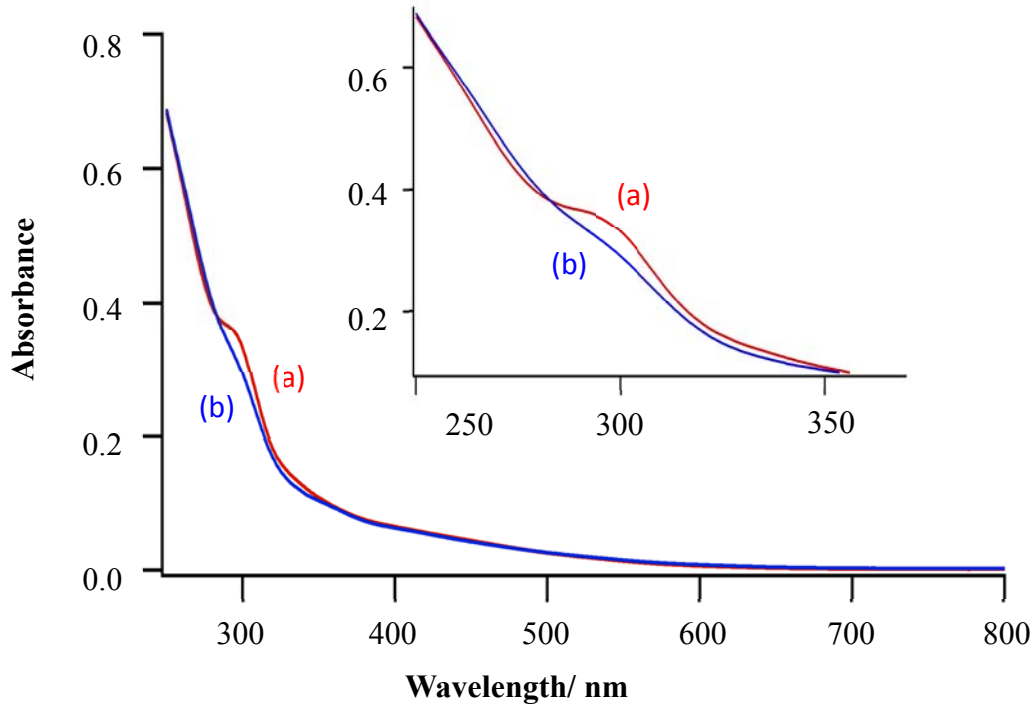

Figure 3.2 A UV-vis spectral change from (a) $[Ni^{II}L(H_2O)(\mu\text{-}H)Ru^{II}(\eta^6\text{-}C_6Me_6)]^+$ (**2**) to (b) $[Ni^{II}L(HCOO)(\mu\text{-}H)Ru^{II}(\eta^6\text{-}C_6Me_6)]$ (**1**).

3.3.2. Crystal of $[Ni^{II}L(HCOO)(\mu\text{-}H)Ru^{II}(\eta^6\text{-}C_6Me_6)]$ (1)

The aqueous solution of [**3**]$(NO_3)_2$ and HCOONa was stood overnight to gradually precipitate brow crystal of **1,** which structured of **1** was determined by X-ray analysis. (Figure 3.3).

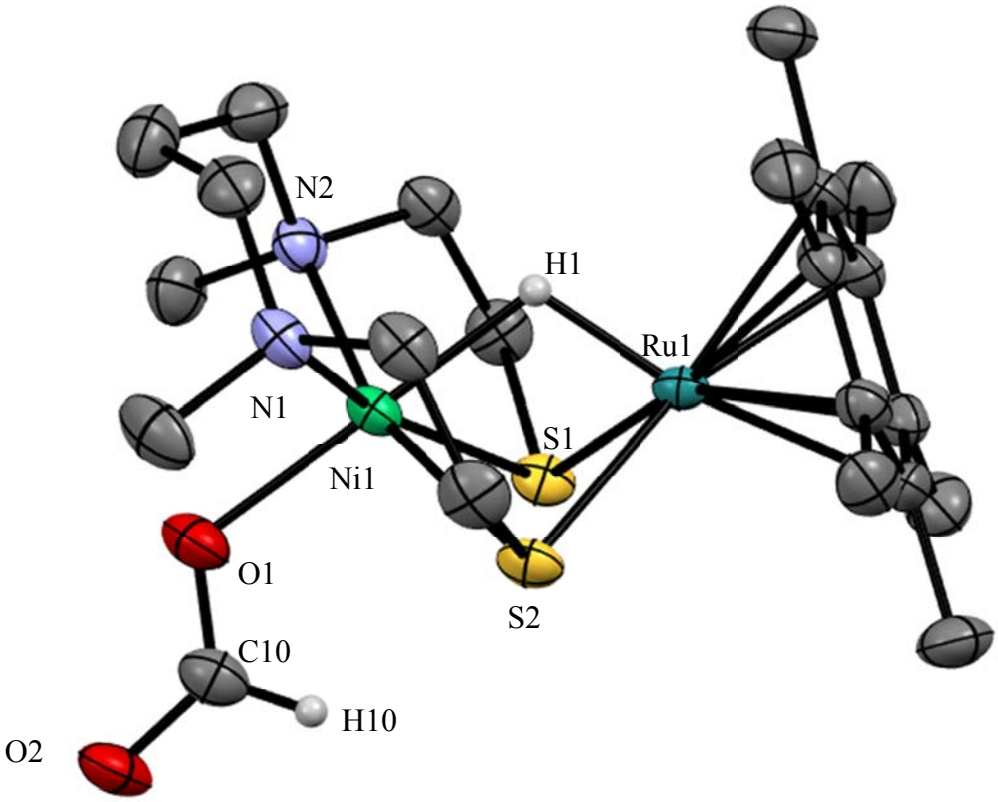

Figure 3.3 An ORTEP drawing of **1** with ellipsoids at 50% probability. The hydrogen atoms of the ligand L (N, N'-dimethyl-3,7-diazanonane-1,8-dithiolato) and C_6Me_6 are omitted for clarity.

The framework of **1** is based around a NiS_2Ru butterfly core with a bridging hydride ion (Figure 3.3). The Ru-H distance (1.610 Å) in Ni(μ-H)Ru moiety of **1** is substantially shorter than the Ru-H distance (1.676 Å) in Ni(μ-H)Ru moiety of [**2**](NO_3) however, the distance of Ni-Ru of **1** (2.7780 Å) is longer than of [**2**](NO_3) (2.739 Å). The Ni atom of **1** adopts distorted octahedral coordination that consists of the hydrido and formato ligands at the axial site and the N_2S_2 donor ligand at the equatorial site. Similar to [**2**](NO_3), the bridging H atom is closer to the Ru atom (Ru-H = 1.610 Å, Ni-H = 1.88 Å) in the Ni(μ-H)Ru moiety of **1**. It is considered that two electrons of Ru-H

unit may be donated to Ni unit through the bridging H atom. The Ni-S-Ru angles are 71.13° and 71.14° for **1** are substantially larger than the Ni-S-Ru angles are 70.7° and 71.14° for [**2**](NO_3). The distance of Ni-O1 of **1** (O of COO^-) is smaller than Ni-O1 of [**2**](NO_3) (O of H_2O).

Table 3.1 Selected bond lengths (Å) and angles (deg) for [**2**](NO_3) and **1**

	[**2**](NO_3)[27]	**1**
Ni-Ru1	2.739(3)	2.7780(11)
Ni1-H1	1.859(7)	1.88(6)
Ni1-O1	2.122(5)	2.060(4)
Ni1-S1	2.359(10)	2.3818(19)
Ni1-S2	2.362(9)	2.3676(19)
Ni1-N1	2.119(3)	2.1256(6)
Ni1-N2	2.117(4)	2.120(6)
Ru1-H1	1.676(8)	1.610(6)
Ru1-S1	2.375(11)	2.3939(17)
Ru1-S2	2.388(7)	2.4084(17)
Ru1-C11	2.229(5)	2.220(6)
Ru1-C12	2.219(5)	2.219(6)
Ru1-C13	2.209(4)	2.219(6)
Ru1-C14	2.261(4)	2.270(6)
Ru1-C15	2.227(4)	2.237(6)
Ru1-C16	2.216(4)	2.225(6)
O1-C10		1.268(9)
O2-C10		1.238(9)
Ni1-S1-Ru1	70.7 (3)	71.13(5)
Ni1-S2-Ru1	70.4(2)	71.14(4)

3.3.3. IR spectrum of $[Ni^{II}L(HCOO)(\mu\text{-}H)Ru^{II}(\eta^6\text{-}C_6Me_6)]$ [1]

An IR spectra of **1** in the region 1000-3000 cm^{-1} region of 1 were presented in Figure 3.4 In the solid state (KBr disk), the peak at 1760 cm^{-1} is assigned to ν(Ni-H-Ru) that shift to 1248 cm^{-1} by isotopic substitution of H with D. Similarly, the peak at 1349 cm^{-1}, which is assigned to δ(C-H of HCOO) shifts to 1329 cm^{-1} by isotopic substitution of H with D.

The results are expected by Hooke's law calculation for Ni-H-Ru and HCOO stretching mode.

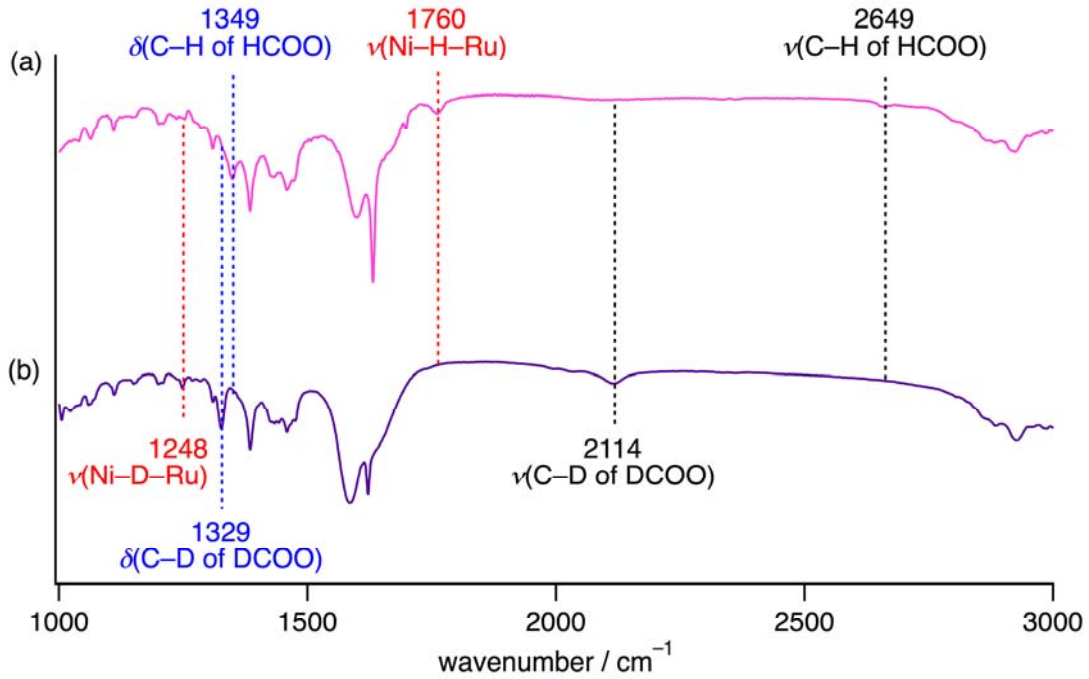

Figure 3.4 IR spectra of (a) $[Ni^{II}L(HCOO)(\mu\text{-}H)Ru^{II}(\eta^6\text{-}C^6Me^6)]$ (**1**) and (b) $[Ni^{II}L(DCOO)(\mu\text{-}D)Ru^{II}(\eta^6\text{-}C_6Me_6)]$ (double D-labelled **1)** as KBr disks. An IR spectrum of **1** shows isotope-sensitive bands at 1349, 1760 and 2649 cm^{-1}, which shift to 1329, 1248 and 2114 cm^{-1}, respectively, after isotopic substitution of H by D in the hydrido and formato positions.

3.3.4. ESI mas spectrum of [Ni^{II}L(HCOO)(μ-H)Ru^{II}(η^6-C_6Me_6)] (1)

Positive- and negative-ion electrospray mass spectrometry (ESI-MS) was used to characterize **1** in an aqueous solution state. A positive-ion ESI mass spectrum of **1** in water exhibits a prominent signal at *m/z* 543.2 {relative intensity (*I*) = 100% in the range m/z 200–2000} (Figure 3.5). The signal has a characteristic isotopic distribution that matches well with the calculated isotopic distribution for [**1**−HCOO]$^+$, which shifts to *m/z* 544.2 by the use of [Ni^{II}L(DCOO)(μ-D)Ru^{II}(η^6-C_6Me_6)] (double D-labelled **1**).

A negative-ion ESI mass spectrum of **1** shows a $HCOO^-$ adduct, which displays a prominent signal at *m/z* 633.2 (*I* = 100% in the range *m/z* 200–2000) (Figure 3.6), whose characteristic isotopic distribution matches well with the calculated isotopic distribution for [**1** + HCOO]$^-$. The signal shifts to *m/z* 636.3 by using double D-labelled **1**.

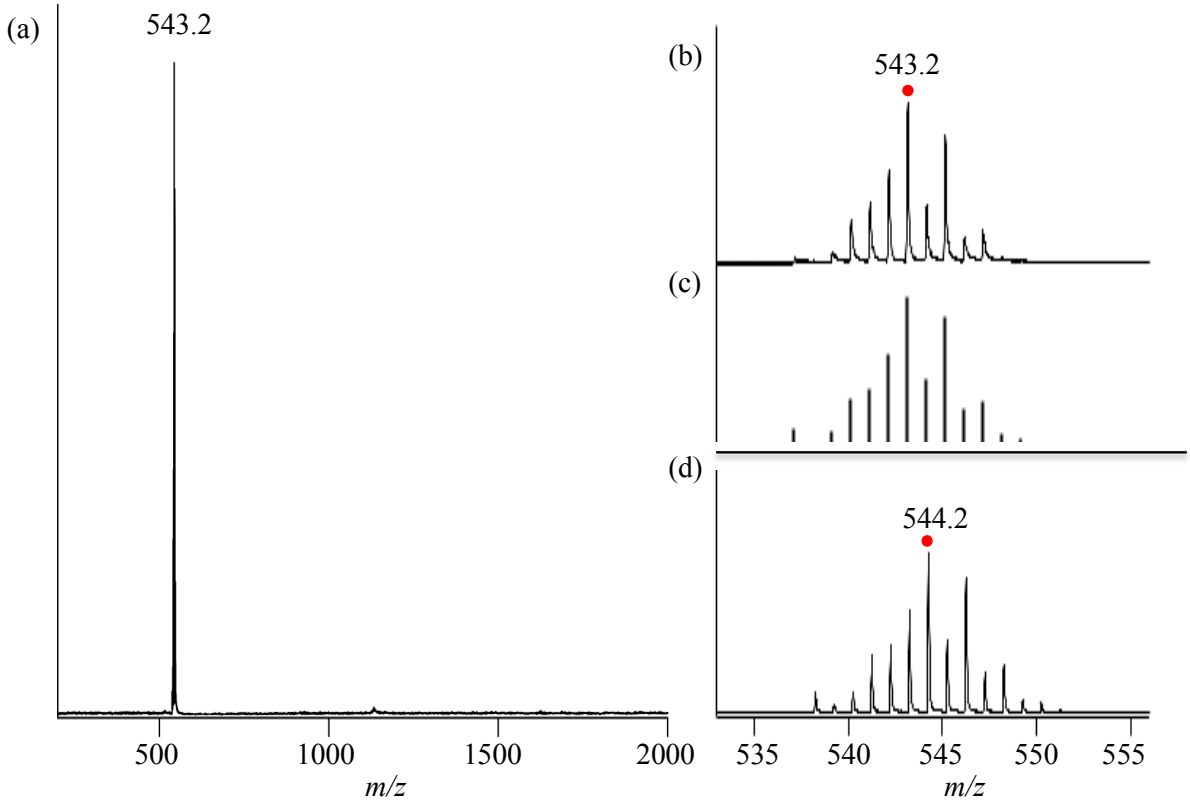

Figure 3.5 (a) A positive-ion ESI mass spectrum of [Ni^{II}L(HCOO)(μ-H)Ru^{II}(η^6-C_6Me_6)] (**1**) in H_2O at pH 7.0. (b) Signal at *m/z* 543.2 corresponds to [**1** – HCOO]$^+$. (c) Calculated isotopic distribution corresponds to [**1** – HCOO]$^+$. (d) A positive-ion ESI mass spectrum of [Ni^{II}L(DCOO)(μ-D)Ru^{II}(η^6-C_6Me_6)] (double D-labelled **1)** in D_2O at pD 7.0. Signal at *m/z* 544.2 corresponds to [double D-labelled **1** – DCOO]$^+$.

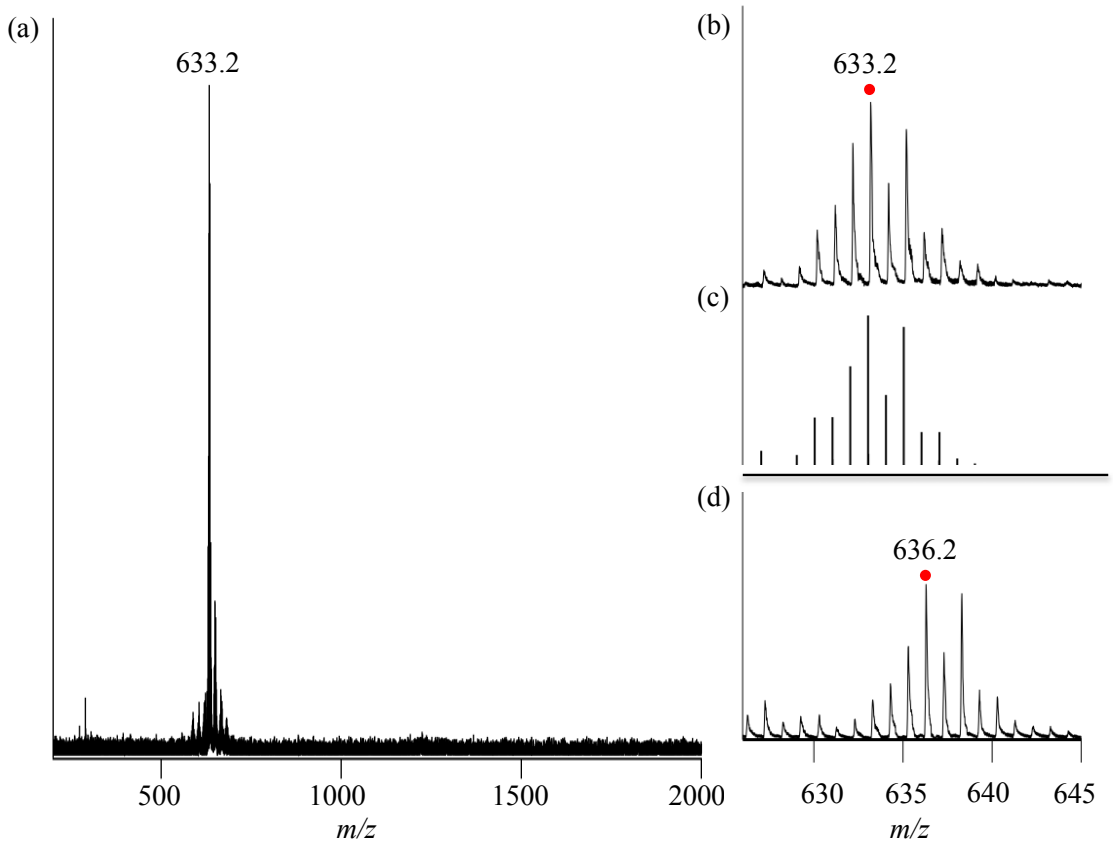

Figure 3.6 (a) A negative-ion ESI mass spectrum of [Ni^{II}L(HCOO)(μ-H)Ru^{II}(η^6-C_6Me_6)] (**1**) in H_2O at pH 7.0. (b) Signal at *m/z* 633.2 corresponds to [**1** + HCOO]$^-$. (c) Calculated isotopic distribution corresponds to [**1** + HCOO]$^-$. (d) A negative-ion ESI mass spectrum of [Ni^{II}L(DCOO)(μ-D)Ru^{II}(η^6-C_6Me_6)] (double D-labelled **1)** in D_2O at pD 7.0. Signal at *m/z* 636.2 corresponds to [double D-labelled **1** + DCOO]$^-$.

3.3.5. Effect of pH on H_2 evolution catalyzed by NiRu complex

The H_2 and CO_2 evolution was catalyzed by the (μ-hydrido)(formato) $Ni^{II}Ru^{II}$ complex **1**, in which the H_2 and CO_2 gases were detected by GC. A pH-dependent profile of turnover numbers (TONs, mol of H_2 evolved/mol of catalyst) of H_2 evolution form HCOOH for 1 h at 60°C was presented in Figure 3.7. The rate of H_2 evolution was carried out in this study shows a maximum of TONs is 857 around pH 3.5. The pH dependence should be explained by a protonation process of a proposed low-valent species **B** (Figure 3.8) and by the stability of the complex, for example, the species is decomposed to unidentified mononuclear species below pH 3.0. It was confirmed that the reaction of **2** with H_2 and CO_2 in H_2O in the range of pH 2.0–9.0 at room temperature did not afford **1**.

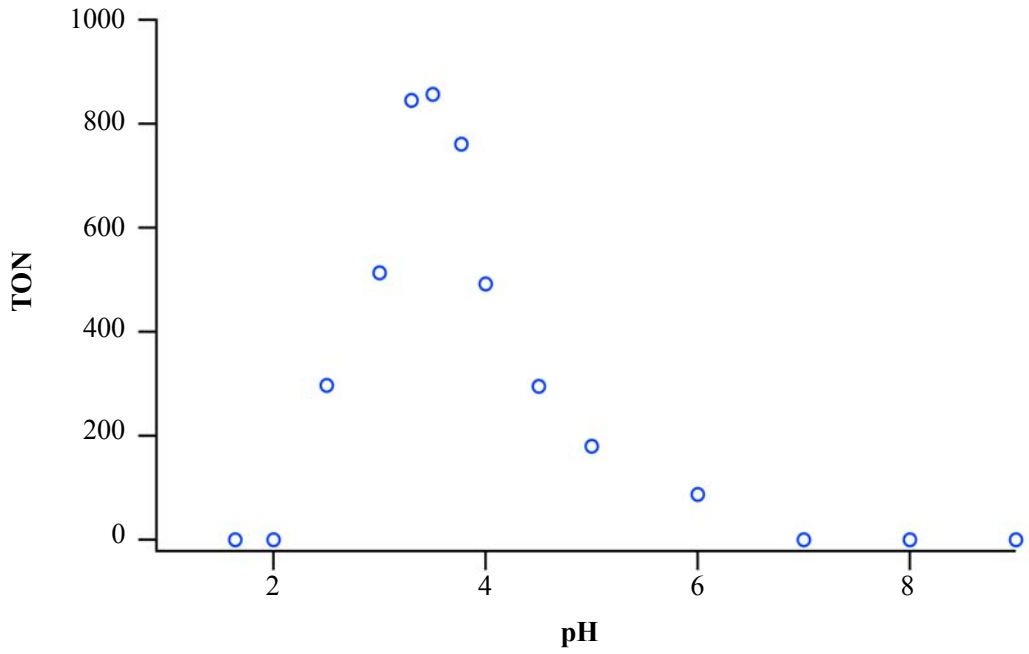

Figure 3.7 pH-dependent H_2 evolution catalyzed by **2** (7.3 nmol) with HCOONa (146 μmol) in water (510 μL) for 1 h at 60°C. The maximum turnover number (TON) is 857 at pH 3.5.

3.3.6 Proposed mechanism of H_2 evolution

Figure 3.8 shows a proposed mechanism for H_2 evolution from HCOOH catalyzed by the (μ-hydrido)(formato) $Ni^{II}Ru^{II}$ complex **1.** The (μ-hydrido)(formato) $Ni^{II}Ru^{II}$ complex **1** is generated by the reaction of the μ-hydrido $Ni^{II}Ru^{II}$ complex with $HCOO^-$. Formation of CO_2 from **1** affords a dihydrido intermediate **A** and then reductive elimination of H_2 from **A** yields the low-valent species **B**. The species **B** reduces H^+ to reform **2**. This reaction mechanism is the same as the H_2 activation mechanism by **2** except that HCOOH is used instead of H_2.[34,35]

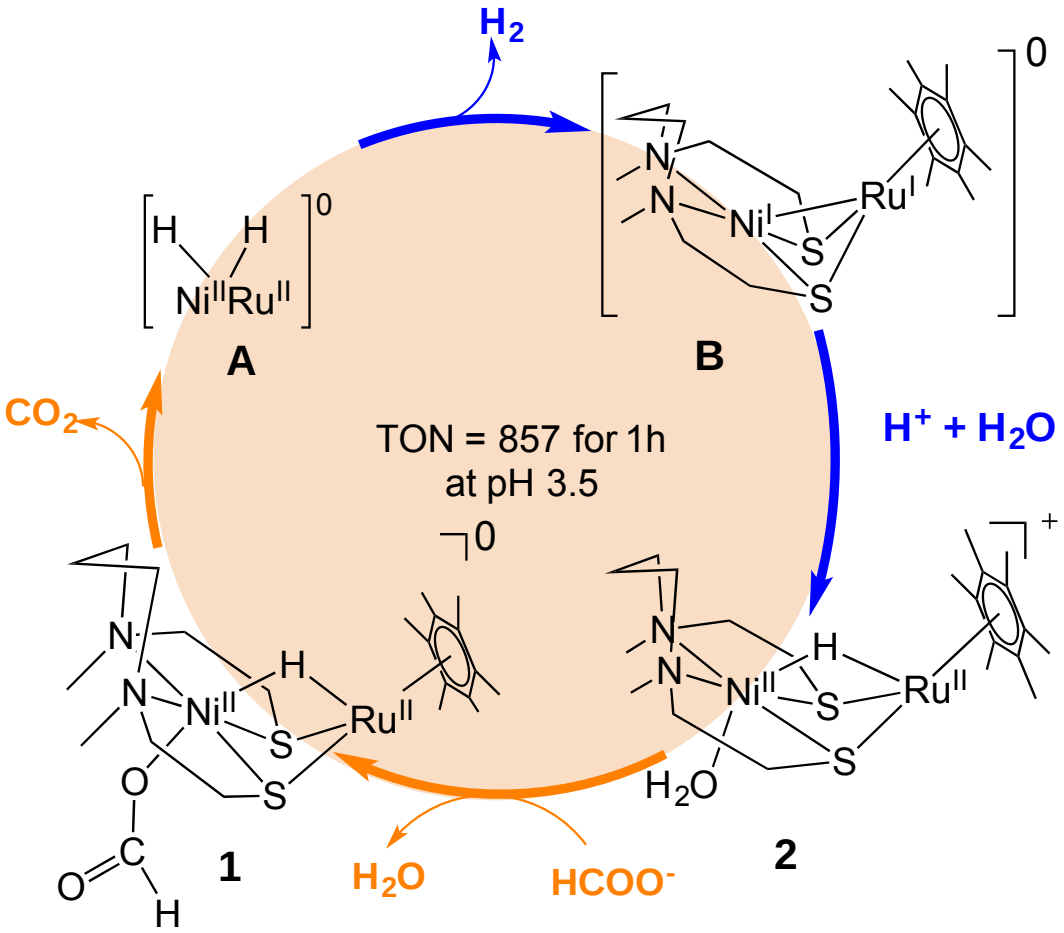

Fig 3.8 A Proposed mechanism of H_2 evolution from HCOOH catalyzed by a NiRu complex in acidic media.

3.4. CONCLUSIONS

We have achieved H_2 evolution from HCOOH catalyzed by a NiRu complexes, which base on [NiFe]H_2ase, without any need for additional energy input. Furthermore, we have structurally defined the reaction intermediate of the (μ-hydrido)(formato) $Ni^{II}Ru^{II}$ complex during catalytic H_2 evolution.

REFERENCES

1. **Steele, B. C.H. and Heinzel, A.**: Material for fuel-cell technology, Nature, **414**, 345-352 (2001).
2. **Veziroğlu, T. N and Şahin, S.**: 21st Century's energy: Hydrogen energy system, Energ. Convers. Manage., **49**, 1820-1831 (2008)..
3. **Dutta S.**: A review on production, storage of hydrogen and its utilization as energy resource, J. Ind. Eng Chem., **20**, 1148-1156 (2014).
4. **Joó, F.**: Breakthroughs in hydrogen storage- formic acid as a sustainable storage material for hydrogen, ChemSusChem, **1**, 805-808 (2008).
5. **Graseman M. and Laurency G.**: Formic acid as a hydrogen source- recent developments and future trends, Energy Environ. Sci., **5**, 8171-8181 (2012).
6. **Enthaler, S., Langermann, J. V., and Schmidt, T.**: Carbon dioxide and formic acid-the couple of environmental-friendly hydrogen storage? Energy Environ. Sci., **3**, 1207-1217 (2010).
7. **Prinske, C., Jaroschinsky M., and Sawers, R. G.**: Levels of control exerted by the Isc iron-sulfur cluster system on biosynthesis of the formate hydrogenlyase complex, Microbiology, **159**, 1179–1189 (2013).
8. **Forzi, L. and Sawers, R. G.**: Maturation of [NiFe]-hydrogenases in *Escherichia coli*, BioMetals, 2007, **20**, 565–578;
9. **Bagramyan, K. and Trchounian, A.**: Structural and functional features of formate hydrogenase lyase, an enzyme of mixed-acid fermentation from *Escherichia coli*, Biochemistry, **68**, 1159–1170 (2003).
10. **Hille, R., Hall, J., and Basu P.**: The molybdenum enzymes, Chem. Rev., **114**, 3963–4038 (2014).

11. **Dobbek, H.**: Structural aspects of mononuclear Mo/W-enzymes, Coord. Chem. Rev., **255**, 1104-1116 (2011).
12. **Gonzalez, P. J., Rivas, M. G., Mota, C. S., Brondino, C. D., Moura, I., and Moura, J. J. G.**: Periplasmic nitrate reductases and formate dehydrogenases: Biological control of the chemical properties of Mo and W for fine tuning of reactivity, substrate specificity and metabolic role, Coord. Chem. Rev., **257**, 315–331(2013).
13. **Lubitz, W., Ogata, H., Rüdiger, O., and Reijerse, E.**: Hydrogenases, Chem. Rev., **114**, 4081–4148 (2014).
14. **Simmons, T. R., Berggren, G., Bacchi, M., Fontecave, M., and Artero, V.**: Mimicking hydrogenases: From biomimetics to artificial enzymes, Coord. Chem. Rev., **270–271**, 127–150 (2014).
15. **Tard, C. and Pickett, C. P.**: Structural and functional analogues of the active sites of the [Fe]-, [NiFe]-, and [FeFe]-Hydrogenases, Chem. Rev., **109**, 2245–2274 (2009).
16. **Gloaguen, F. and Rauchfuss, T. B.**: Small molecule mimics of hydrogenases: hydrides and redox, Chem. Soc. Rev., **38**, 100–108 (2008).
17. **DuBois, M. R. and DuBois, D. L.**: The roles of the first and second secoordination spheres in the design of the molecular catalysts for H_2 production and oxidation, Chem. Soc. Rev., **38,** 62–72 (2008).
18. **Armstrong, F. A., Belsey, N. A., Cracknell, J. A., Goldet, G., Parkin, A., Reisner, E., Vincent, K. A., and Wait, F. W.**: Dynamic electrochemical investigations of hydrogen oxidation and production by enzymes and implications for future technology, Chem. Soc. Rev., **38**, 36–51 (2008).

19. **Fontecilla-Camps, J. C., Volbeda, A., Cavazza, C., and Nicolet, Y.**: Structure/function relationships of [NiFe]- and [FeFe]-hydrogenases, Chem. Rev., **107**, 4273–4303 (2007).
20. **Vignais, M. V. and Billoud, B.**: Occurrence, classification, and biological function of hydrogenases: An overview, Chem. Rev., **107**, 4206–4272 (2007).
21. **Kubas, G.**: Fundamentals of H_2 binding and reactivity on transition metals underlying hydrogenase functional and H_2 production and storage, Chem. Rev., **107**, 4152–4205 (2007).
22. **Georgakaki, I. P., Thomson, L. M., Lyon, E. J., Hall, M. B., and Darensbourg, Y.**: Fundamental properties of small molecule models of Fe-only hydrogenase: computations relative to the definition of an entatic state in the active site, Coord. Chem. Rev., **238–239**, 255–266 (2002).
23. **Ogo, S., Ichikawa, K., Kishima, T., Matsumoto, T., Nakai, H., Kusaka, K., and Ohhara, K.**: A functional [NiFe]hydrogenase mimic that catalyzes electron and hydride transfer from H_2, Science, **339**, 682–684 (2013).
24. **Boyington, J. C, Gladyshev, V. N., Khangulov, S. V., Stadtman, T. C., and Sun, P. D.**: Crystal structure of formate dehydrogenase H: catalysis involving Mo, molybdopterin, selenocysteine, and a Fe_4S_4 cluster, Science, **275**, 1305-1308 (1997).
25. **Barton, B. E. and Rauchfuss, T. B.**: Hydride-containing models for the active site of the nickel-iron hydrogenases, J. Am. Chem. Soc., **132**, 14877–14885 (2010).
26. **Summers, P. A., Dawson, J., Ghiotto, F., Hanson-Heine, M. W. D., Vuong, K. Q., Davies, E. S., Sun, X.-Z, Besley, N. A., McMaster, J., George, M. W., and**

Schröder, M.: Photochemical dihydrogen production using an analogue of the active site of [NiFe] hydrogenase, Inorg. Chem., **53**, 4430–4439 (2014).

27. **Ogo, S., Kabe, R., Uehara, K., Kure, B., Nishimura, T., Menon, S. C., Harada, R., Fukuzumi, S., Higuchi, Y., Ohhara, T., Tamada, T., and Kuroki, R.**: A Dinuclear Ni(μ-H)Ru complex derived from H_2, Science, **316**, 585–587 (2007).
28. **Wang, W.,-H., Himeda, Y., Muckerman, J. T., and Fujita, E.**: Interconversion of CO_2/H_2 and formic acid under mild conditions in water: ligand design for effective catalysis, Adv. Inorg. Chem., **66**, 189–222 (2014).
29. **Fujita, E., Muckerman, J. F., and Himeda, Y.**: Interconversion of CO_2 and formic acid by bio-inspired Ir complexes with pendent bases, Biochim. Biophys. Acta., **1827**, 1031–1038 (2013).
30. **Appel, A. M., Bercaw, J. E., Bocarsly, A. B., Dobbek, H., DuBois, D. L., M. Dupuis, Ferry, J. G., Fujita, E., Hille, R., Kenis, P. J. A., Kerfeld, C. A., Morris, R. H., Peden, C. H. F., Portis, A. R., Ragsdale, S. W., Rauchfuss, T. B., Reek, J. N. H., Seefeldt, L. C., Thauer, R. K., and Waldrop, G. L.**: Frontiers, opportunities, and challenges in biochemical and chemical catalysis of CO_2 fixation, Chem. Rev., **113**, 6621–6658 (2013).
31. **Fukuzumi, S. and Suenobu, T.**: Hydrogen storage and evolution catalyzed by metal hydride complexes, Dalton Trans., **42**, 18–28 (2013).
32. **Glosoe, P. K. and Long, F. A.**: Use of glass electrodes to measure acidities in deuterium oxide, J. Phys. Chem., **64**, 188-190 (1960).
33. **Mikkelsen, K. and Nielsen, S. O.**: Acidity measurements with the glass electrode in H_2O-D_2O mixtures, J. Phys. Chem., **64**, 632-637 (1960).

34. **Ogo, S.**: H_2 and O_2 activation-a remarkable insight into hydrogenase, Chem. Rec., **14**, 397–409 (2014).

35. **Ogo, S.**: Electrons from hydrogen, Chem. Commun., 3317–3325 (2009).

CHAPTER 4

CONCLUDING REMARKS

The original concept of my studies is to create the fusion technology by developing useful biological- and chemical- catalysts into the idea system, which can be used as an energy generator to produce "H_2" or activation of "formate". Therefore, I have focused on the development of a new biological and its mimetic catalysts. In this thesis, I have successfully purified and characterized a new formate dehydrogenase from our newly isolated bacterium *Citrobacter* sp. S-77. In addition, I have attempted to create the model complex of formate hydrogen lyase with the modified [NiFe]H_2ase model complex. In this Chapter, I summarized the main results and key findings in the concluding remarks.

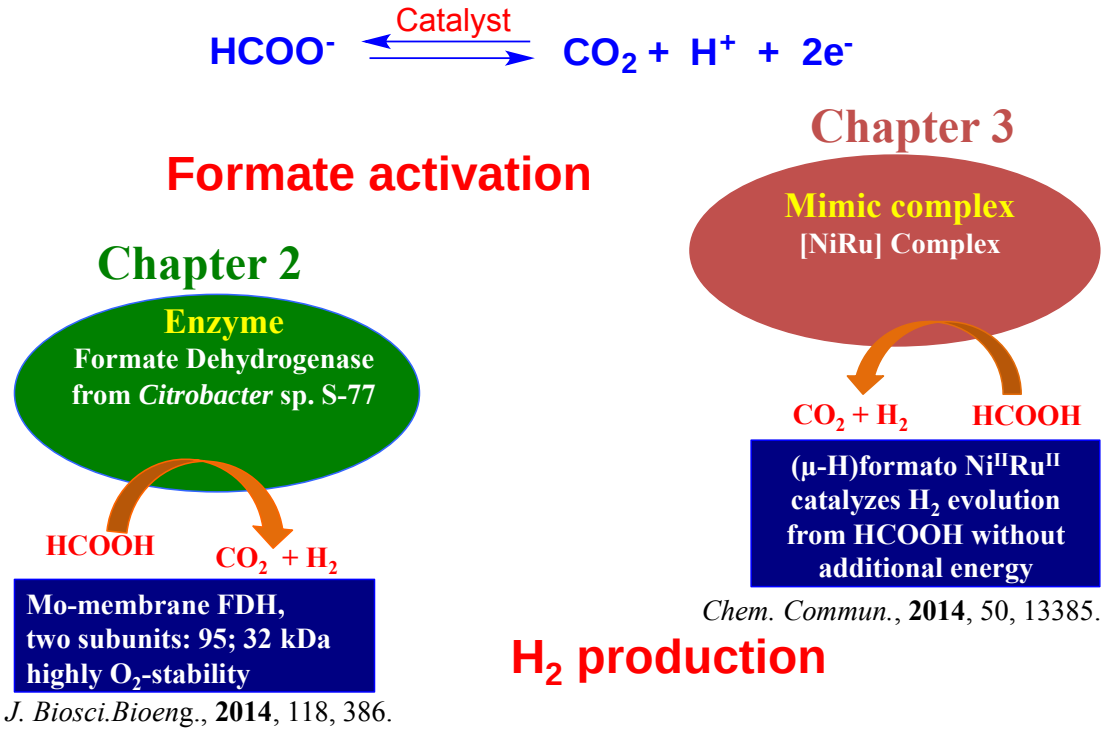

Figure 4.1 Harmonized system between biological and chemical catalysts for application of renewable energy system.

Chapter 2

This study has attempted to find a new robust formate oxidizing enzymes from newly isolated bacteria from extreme environments. During the course of the studies, I found an O_2-stable membrane-bound formate dehydrogenase from the newly isolated bacterium *Citrobacter* sp. strain S-77. The strain was isolated from the water samples of a tepid spring at Aso-Kuju National Park, Kumamoto, Japan. In the previously studies, we have found another novel enzyme of a membrane-bound [NiFe]hydrogenase from the same bacterium. The MBH plays an effective anode catalyst for H_2 oxidation in polymer electrolyte fuel cell. Like the MBH, the purified FDH is a molybdenum-containing enzyme, displaying a remarkable O_2-stability along with thermostability and a wide range of pH resistance. The purified FDH_{S77} was not contained a heme *b* subunit.

The maximal activity (V_{max}) for formate oxidation at 30°C was 30.4 U/mg using benzyl viologen as an electron acceptor. This report is the first purification and characterization of a molybdenum containing FDH from the genus of *Citrobacter*. This newly found O_2-stable FDH_{S77} might be an important enzyme, which has a great potential for use as a biocatalyst in industrial applications.

Chapter 3

In order to develop the model system of FHL protein complex, I synthesized the (μ-hydrido)(formato) $Ni^{II}Ru^{II}$ complex $[Ni^{II}L(HCOO)(\mu\text{-}H)Ru^{II}(\eta^6\text{-}C_6Me_6)]$, based on the [NiFe]hydrogenase model. The new model complex can effectively catalyze the oxidation of formic acid to H_2 and CO_2. The NiRu complex was developed by Ogo group is also capable of dihydrogen oxidation both directions of the cleavage and production of H_2. This is the first example of H_2 production using the mimic [NiFe]H_2ase. The catalytic reaction of the complex is not required for any additional energy. The FHL model complex may has function as an effective catalyst for H_2 production.

Taking these results together, the novel catalysts of the robust FDH and the FHL model complex have many potential abilities to be used as an efficient catalyst in H_2-based technology. The results described in this thesis should provide new insight into the development of the more effective biocatalysts and bio-inspired model complexes for formate activation and H_2 production, which may contribute to improved H_2-based technology.

List of Publications

Chapter 2

Molybdenum-containing membrane-bound formate dehydrogenase isolated from Citrobacter sp. S-77 having high stability against oxygen, pH, and temperature

Nguyen, N. T., Yatabe, T., Yoon, K.-S., Ogo, S.

J. Biosci. Bioeng., **2014**, 118, 386-391

Chapter 3

A [NiFe]hydrogenase model that catalyses the release of hydrogen from formic acid

Nguyen, N. T., Mori, Y., Matsumoto, T., Yatabe T., Kabe, R., Nakai, H., Yoon, K.-Y, Ogo, S.

Chem. Commum., **2014**, 50, 13385-13387

Acknowledgements

I would like to express my sincere gratitude to my advisor Professor **Seiji Ogo** for his guidance, caring, patience, enthusiasm, and immense knowledge. He always provides me with an excellent atmosphere for doing research.

My sincere thanks also go to Professor **Yoshio Hisaeda** and Professor **Noriho Kamiya** for their encouragement, helpful comments, and advise.

I desires to express my thanks to Associate Professor **Ki-Seok Yoon,** Associate Professor **Takahiro Matsumoto**, and Assistant Professor **Takeshi Yatabe** for their guidance me in all the time of research and writing of this thesis, and helping me to develop my background in biochemistry and organic chemistry.

I would like to thank Associate Professor **Hidetaka Nakai** and Dr. **Masatatsu Suzuki** for their supported and useful suggestions.

I also would like to thank Dr. **Kiyoshi Isobe** for his warmness encouragement and useful suggestions at beginning of my life in Japan and Ogo Lab.

I also wish to thanks to Ms. **Yukiko Shigematsu** for her assistance and encouragement.

I would like to thank Dr. **Kyoshiro Nonaka**, who as a good tutor was always willing to help and give his best suggestions my works in laboratory and outside.

Many thanks I would like to give for the all members of Ogo laboratory.

My thanks also give to all my friends who study and work in Kyushu University, thanks to always stand by my side, made me do not feel lonely during all time I stay here.

At the end, I would like express appreciation to my family and my friends for all of the sacrifices that you have made on my behalf. Your prayer for me was what supported me, and incented me to strive towards my good.

Nguyen Thi Thanh Nga

Jan 14, 2015
Fukuoka, Japan